

1     **A non-equilibrium model for soil heating and moisture transport during**  
2                                   **extreme surface heating**

3                                   W. J. Massman  
4                                   USDA Forest Service  
5                                   Rocky Mountain Research Station  
6                                   240 West Prospect  
7                                   Fort Collins, CO 80526 USA  
8                                   email: [wmassman@fs.fed.us](mailto:wmassman@fs.fed.us)

9                                   June 2015

10 **Abstract.** With increasing use of prescribed fire by land managers and increasing likelihood  
11 of wildfires due to climate change comes the need to improve modeling capability of extreme  
12 heating of soils during fires. This issue is addressed here by developing a one-dimensional  
13 non-equilibrium (liquid-vapor phase change) model of soil evaporation and transport of heat,  
14 soil moisture, and water vapor, for use with surface forcing ranging from daily solar cycles  
15 to extreme conditions encountered during fires. The model employs a linearized Crank-  
16 Nicolson scheme for the conservation equations of energy and mass and its performance is  
17 evaluated against dynamic soil temperature and moisture observations obtained during lab-  
18 oratory experiments on soil samples exposed to surface heat fluxes ranging between 10,000  
19 and 50,000  $\text{Wm}^{-2}$ . The Hertz-Knudsen equation is the basis for constructing the model's  
20 non-equilibrium evaporative source term. Some unusual aspects of the model that were found  
21 to be extremely important to the model's performance include: (1) a dynamic (temperature  
22 and moisture potential dependent) condensation coefficient associated with the evaporative  
23 source term, (2) an infrared radiation component to the soil's thermal conductivity, (3) a  
24 dynamic residual soil moisture, which is parameterized as a function of temperature and soil  
25 water potential and incorporated into the water retention curve and hydraulic conductivity  
26 functions with the intent of allowing the model to better capture some of the dynamic aspects  
27 of the strongly bound soil moisture that seems to require temperatures well beyond 150 C  
28 to fully evaporate. The model also can be configured to include film flow, although this phe-  
29 nomenon did not contribute much to the model's overall performance. In general, the model  
30 simulates the laboratory-observed temperature dynamics quite well, but is less precise (but  
31 still good) at capturing the moisture dynamics. The model emulates the observed increase  
32 in soil moisture ahead of the drying front and the hiatus in the soil temperature rise during  
33 the strongly evaporative stage of drying. It also captures the observed rapid evaporation of  
34 soil moisture that occurs at relatively low temperatures (50-90 C), and can provide quite

35 accurate predictions of the total amount of soil moisture evaporated during the laboratory  
36 experiments. The model's solution for water vapor density (and vapor pressure), which can  
37 exceed one standard atmosphere, cannot be experimentally verified, but they are supported  
38 by results from (earlier and very different) models developed for somewhat different purposes  
39 and for different porous media. Overall, this non-equilibrium model provides a much more  
40 physically realistic simulation over a previous equilibrium model developed for the same pur-  
41 pose. Current model performance strongly suggests that it is now ready for testing under  
42 field conditions.

## 43 1. Introduction

44 Since the development of the theory of Philip and de Vries (PdV model) almost 60  
45 years ago [*Philip and de Vries* 1957; *de Vries* 1958] virtually all models of evaporation and  
46 condensation in unsaturated soils have assumed that soil water vapor at any particular depth  
47 into the soil is in equilibrium with the liquid soil water (or soil moisture) at the same depth.  
48 (Note: such soil evaporation models also assume thermal equilibrium, so that at any given  
49 depth the mineral soil, the soil moisture, and the soil air and water vapor within the pore  
50 space are also at the same temperature.) In essence, this local equilibrium assumption means  
51 that whenever the soil moisture changes phase it does so instantaneously. This assumption  
52 is quite apropos for its original application, which was to describe the coupled heat and  
53 moisture transport in soils (and soil evaporation in particular) under environmental forcings  
54 associated with the daily and seasonal variations in radiation, temperature, precipitation,  
55 etc. [e.g., *Milly* 1982; *Novak* 2010; *Smits et al.* 2011]. Under these conditions assuming local  
56 equilibrium is reasonable because the time required to achieve equilibrium after a change of  
57 phase is ‘instantaneous’ when compared to the time scale associated with solar and other  
58 normal environmental forcings. The great benefit to the equilibrium assumption is that for  
59 modeling purposes it is a significant simplification to the equations that describe heat and  
60 moisture flow in soils because it eliminates the need to include soil water vapor density,  $\rho_v$ ,  
61 as an independent model variable. More formally, under equilibrium  $\rho_v$  is directly equated  
62 to the equilibrium vapor density, which is a function only of local soil temperature and soil  
63 water content (or more specifically the soil water potential).

64 Subsequent to the development of the original PdV model the equilibrium assumption  
65 has also been incorporated into models of heat and moisture transport (evaporation and  
66 condensation) in soils and other porous media under more extreme forcings associated with  
67 high temperatures and heat fluxes. For example, it has been applied to (*i*) soils during

68 wildfires and prescribed burns [*Aston and Gill* 1976; *Campbell et al.* 1995; *Durany et al.*  
69 2010; *Massman* 2012], (ii) drying of wood [*Whitaker* 1977; *di Blasi* 1997], (iii) drying and  
70 fracturing of concrete under high temperatures [*Dayan* 1982; *Dal Pont et al.* 2011], (iv)  
71 high temperature sand-water-steam systems [e.g., *Udell* 1983; *Bridge et al.* 2003], and (v)  
72 evaporation of wet porous thermal barriers under high heat fluxes [*Costa et al.* 2008].

73 Although the PdV model and the equilibrium assumption have certainly led to many  
74 insights into moisture and vapor transport and evaporation in porous media, it has, nonethe-  
75 less, yielded somewhat disappointing simulations of the coupled soil moisture dynamics dur-  
76 ing fires [see *Massman* 2012 for further details and general modeling review]. Possibly the  
77 most interesting of these modeling “disappointments” is provided by soil/fire-heating model  
78 of *Massman* [2012], who found that as the soil moisture evaporated it just re-condensed  
79 and accumulated ahead of the dry zone, so that no water actually escaped the soil at all  
80 (which, to say the least, seems physically implausible)! He further traced the cause of this  
81 anomalous behavior to the inapplicability of the equilibrium evaporation assumption, which  
82 allowed the soil vapor gradient behind the drying front to become so small that the soil  
83 vapor could not escape (diffuse) out of the soil. Or, more fundamentally, the calculated  
84 vapor and its attendant gradient became largely meaningless because it is impossible for  
85 water vapor to be in equilibrium with liquid water if there is no liquid water. Of course,  
86 such extremely dry conditions are just about guaranteed during soil heating events like fires.  
87 *Novak* [2012] also recognized the inapplicability of the equilibrium assumption for very dry  
88 soils, but under more normal environmental forcing. On the other hand, even under normal  
89 (and much less extreme) soil moisture conditions both *Smits et al.* [2011] and *Ouedraogo*  
90 *et al.* [2013] suggest that non-equilibrium formulations of soil evaporation may actually im-  
91 prove model performance, which implies that the non-equilibrium assumption may really be  
92 a more appropriate description for soil evaporation and condensation than the equilibrium

93 assumption. The present study is intended to provide the first test of the non-equilibrium  
94 hypothesis during extreme conditions.

95 Specifically, the present study develops and evaluates a non-equilibrium (liquid-vapor  
96 phase change) model for simulating coupled heat, moisture, and water vapor transport during  
97 extreme heating events. It also assumes thermal equilibrium between the soil solids, liquid,  
98 and vapor. It uses a systems-theoretic approach [e.g., *Gupta and Nearing 2014*] focused more  
99 on physical processes than simply tuning model parameters, which here means that whatever  
100 model or parameter “tuning” does occur it is intended to keep the model numerically stable  
101 and as physically realistic as possible.

102 In addition, the present study (model) is a companion to *Massman* [2012]. It uses much  
103 of the same notation as the earlier study. But, unlike its predecessor, this study allows for  
104 the possibility of liquid water movement (i.e., it includes a hydraulic conductivity function  
105 for capillary and film flow). It also improves on and corrects (where possible and as noted in  
106 the text) the mathematical expressions used in the previous paper to parameterize the high  
107 temperature dependency of latent heat of vaporization, saturation vapor density, diffusivity  
108 of water vapor, soil thermal conductivity, water retention curve, etc. This is done in order to  
109 achieve the best representation of the physical properties of water (liquid and vapor) under  
110 high temperatures and pressures [see, e.g., *Harvey and Friend 2004*]. And lastly, in order to  
111 facilitate comparing the present model with the earlier companion model the present study  
112 displays all graphical results in a manner very similar to those of *Massman’s* [2012].

## 113 **2. Model Development**

114 The present model is one-dimensional (in the vertical) and is developed from three coupled  
115 partial differential equations and assumes that the soil liquid and vapor concentrations are  
116 not necessarily in local equilibrium during evaporation/condensation, but that they are in  
117 local thermal equilibrium during any phase change. Consequently the present model has

118 three simulation variables: soil temperature ( $\equiv T$  [C] or  $T_K$  [K]); soil water potential ( $\equiv \psi$   
 119 [J kg<sup>-1</sup>] or  $\psi_n \equiv$  normalized soil water potential [*dimensionless*], where  $\psi_n = \psi/\psi_*$  and  $\psi_* =$   
 120  $-10^6$  [J kg<sup>-1</sup>], which *Campbell et al.* [1995] identify as the water potential for oven dry soil);  
 121 and vapor density ( $\equiv \rho_v$  [kg m<sup>-3</sup>]). This current model employs a linearized Crank-Nicolson  
 122 [C-N] finite difference scheme, whereas the preceding (companion) model [*Massman* 2012]  
 123 used the Newton-Raphson method for solving the fully implicit finite difference equations.  
 124 The present model further improves on its companion by including the possibility of soil water  
 125 movement (hydraulic conductivity function driven by a gradient in soil moisture potential)  
 126 and better parameterizations of thermophysical properties of water and water vapor to allow  
 127 for large variations in the amount of soil water vapor, which *Massman's* [2012] results suggest  
 128 might approach or exceed one standard atmosphere and therefore could become the major  
 129 component of the soil atmosphere during a heating event. This is quite unlike any other  
 130 model of soil heat and moisture flow, which universally assume that dry air is the dominant  
 131 component of the soil atmosphere and that water vapor is a relatively minor component.  
 132 Finally, and also atypical of most other soil models, the model's water retention curve and  
 133 hydraulic function include a dynamic residual soil moisture content as a function of soil  
 134 temperature and soil water potential.

## 135 2.1 Conservation Equations

136 The conservation of thermal energy is expressed as:

$$C_s \frac{\partial T}{\partial t} - \frac{\partial}{\partial z} \left[ \lambda_s \frac{\partial T}{\partial z} \right] + (\eta - \theta) \rho_a c_{pa} u_{vl} \frac{\partial T}{\partial z} = -L_v S_v \quad (1)$$

137

138 where  $t$  [s] is time;  $z$  [m] is soil depth (positive downward);  $T$  is soil temperature in Celsius;  
 139  $C_s = C_s(\theta, T)$  [J m<sup>-3</sup> K<sup>-1</sup>] is the volumetric heat capacity of soil, a function of both soil  
 140 temperature and soil volumetric water content  $\theta$  [m<sup>3</sup>m<sup>-3</sup>];  $\lambda_s = \lambda_s(\theta, T, \rho_v)$  [W m<sup>-1</sup> K<sup>-1</sup>]

141 is the thermal conductivity of the soil, a function of soil temperature, soil moisture, and  
 142 soil vapor density;  $\eta$  [ $\text{m}^3\text{m}^{-3}$ ] is the total soil porosity from which it follows that  $(\eta - \theta)$  is  
 143 the soil's air filled porosity;  $\rho_a = \rho_a(T_K, \rho_v)$  [ $\text{kg m}^{-3}$ ] is the mass density of the soil air, a  
 144 function of temperature and soil vapor density;  $c_{pa} = c_{pa}(T_K, \rho_v)$  [ $\text{J kg}^{-1} \text{K}^{-1}$ ] is specific heat  
 145 capacity of ambient air, also a function of temperature and vapor density;  $u_{vl}$  [ $\text{m s}^{-1}$ ] is the  
 146 advective velocity induced by the change in volume associated with the rapid volitalization  
 147 of soil moisture (detailed below);  $L_v = L_v(T_K, \psi)$  [ $\text{J kg}^{-1}$ ] is the latent heat of vaporization;  
 148 and  $S_v = S_v(T_K, \theta, \psi, \rho_v)$  [ $\text{kg m}^{-3} \text{s}^{-1}$ ] is the source term for water vapor.

149 The conservation of mass for liquid water is

$$\frac{\partial(\rho_w\theta)}{\partial t} - \frac{\partial}{\partial z} \left[ \rho_w K_n \frac{\partial\psi_n}{\partial z} + \rho_w K_H - \rho_w V_{\theta,surf} \right] = -S_v \quad (2)$$

150

151  $\rho_w = \rho_w(T_K)$  [ $\text{kg m}^{-3}$ ] is the density of liquid water;  $K_n = K_n(T_K, \psi, \theta)$  [ $\text{m}^2 \text{s}^{-1}$ ] is the  
 152 hydraulic diffusivity;  $K_H = K_H(T_K, \psi, \theta)$  [ $\text{m s}^{-1}$ ] is the hydraulic conductivity; and  $V_{\theta,surf} =$   
 153  $V_{\theta,surf}(T_K, \theta)$  [ $\text{m s}^{-1}$ ] is the velocity of liquid water associated with surface diffusion of water,  
 154 which may be significant at high temperatures [e.g., *Kapoor et al.* 1989; *Medveď and Černý*  
 155 2011]. Note that switching variables from  $\psi < 0$ , to  $\psi_n$  produces  $\psi_n > 0$  and  $K_n < 0$ .

156 This last equation can be simplified to

$$\rho_w \frac{\partial\theta}{\partial t} - \rho_w \frac{\partial}{\partial z} \left[ K_n \frac{\partial\psi_n}{\partial z} + K_H - V_{\theta,surf} \right] = -S_v \quad (3)$$

157

158 because  $\frac{1}{\rho_w} \frac{d\rho_w}{dT}$  varies by only 4% between about 10 C to 100 C the derivatives  $\frac{\partial\rho_w}{\partial t} \equiv \frac{d\rho_w}{dT} \frac{\partial T}{\partial t}$   
 159 and  $\frac{\partial\rho_w}{\partial z} \equiv \frac{d\rho_w}{dT} \frac{\partial T}{\partial z}$  can be ignored. But the model does retain the temperature dependency  
 160  $\rho_w = \rho_w(T_K)$ , except as noted in the section below on volumetric specific heat capacity of  
 161 soil, and it also specifically includes  $d\rho_w/dT$  for other components of the model.



162 The conservation of mass for water vapor is

$$\frac{\partial(\eta - \theta)\rho_v}{\partial t} - \frac{\partial}{\partial z} \left[ D_{ve} \frac{\partial \rho_v}{\partial z} - (\eta - \theta)u_{vl}\rho_v \right] = S_v \quad (4)$$

163

164 where  $D_{ve} = D_{ve}(T_K, \psi, \rho_v)$  [ $\text{m}^2 \text{s}^{-1}$ ] is the (equivalent) molecular diffusivity associated with  
165 the diffusive transport of water vapor in the soil's air-filled pore space.

166 The final model equations are expressed in terms of the model variables  $(T, \psi_n, \rho_v)$  and  
167 result from: (a) expanding the spatial derivative  $\frac{\partial K_H}{\partial z}$  in terms of the spatial derivatives  $\frac{\partial T}{\partial z}$   
168 and  $\frac{\partial \psi_n}{\partial z}$ , (b) allowing for  $\theta = \theta(\psi_n, T_K)$ , (c) combining Equation (3) with (1) and Equation  
169 (4) with (3), and (d) simplifying Equation (4). These equations are

$$\begin{aligned} (C_s - L_v\rho_w D_{\theta T}) \frac{\partial T}{\partial t} - \frac{\partial}{\partial z} \left[ \lambda_s \frac{\partial T}{\partial z} \right] + \left[ (\eta - \theta)\rho_a c_{pa} u_{vl} + L_v\rho_w \frac{\delta K_H}{\delta T_K} \right] \frac{\partial T}{\partial z} + L_v\rho_w \frac{\partial}{\partial z} \left[ K_m \frac{\partial T}{\partial z} \right] \\ - L_v\rho_w D_{\theta\psi} \frac{\partial \psi_n}{\partial t} + L_v\rho_w \frac{\partial}{\partial z} \left[ K_n^* \frac{\partial \psi_n}{\partial z} \right] + L_v\rho_w \left[ \frac{\partial K_H}{\partial \psi_n} \right] \frac{\partial \psi_n}{\partial z} = 0 \end{aligned} \quad (5)$$

170

171

172 which is the conservation of energy;

$$\begin{aligned} \rho_w D_{\theta T} \frac{\partial T}{\partial t} - \rho_w \frac{\partial}{\partial z} \left[ K_m \frac{\partial T}{\partial z} \right] - \rho_w \left[ \frac{\delta K_H}{\delta T_K} \right] \frac{\partial T}{\partial z} \\ + \rho_w D_{\theta\psi} \frac{\partial \psi_n}{\partial t} - \rho_w \frac{\partial}{\partial z} \left[ K_n^* \frac{\partial \psi_n}{\partial z} \right] - \rho_w \left[ D_{\theta\psi} \frac{\partial K_H}{\partial \theta} \right] \frac{\partial \psi_n}{\partial z} \end{aligned}$$

173

$$+ (\eta - \theta) \frac{\partial \rho_v}{\partial t} - \frac{\partial}{\partial z} \left[ D_v \frac{\partial \rho_v}{\partial z} - (\eta - \theta)u_{vl}\rho_v \right] = 0 \quad (6)$$

174

175 which is the conservation of soil moisture; and

$$-\rho_v D_{\theta T} \frac{\partial T}{\partial t} + (\eta - \theta) \frac{\partial \rho_v}{\partial t} - \frac{\partial}{\partial z} \left[ \mathcal{D}_v \frac{\partial \rho_v}{\partial z} - (\eta - \theta) u_{vl} \rho_v \right] - \rho_v D_{\theta \psi} \frac{\partial \psi_n}{\partial t} = S_v \quad (7)$$

176

177 which is the conservation of mass for water vapor.

178 Apropos to these last three equations: (i)  $D_{\theta \psi} = \partial \theta / \partial \psi_n$  and  $D_{\theta T} = \partial \theta / \partial T_K$  are obtained  
 179 from the water retention curve (WRC); (ii)  $\frac{\delta K_H}{\delta T_K} = \left[ \frac{\partial K_H}{\partial T_K} + \frac{\partial K_H}{\partial \theta} D_{\theta T} \right]$ ; (iii)  $K_m$  [ $\text{m}^2 \text{s}^{-1} \text{K}^{-1}$ ]  
 180 and  $K_n^*$  [ $\text{m}^2 \text{s}^{-1}$ ] (which subsumes  $K_n$ ) are related to  $V_{\theta, surf}$  and are defined in a later section;  
 181 (iv) because  $\rho_v \ll \rho_w$  the term  $(\rho_w - \rho_v) \frac{\partial \theta}{\partial t}$  originally in Equation (6) has been approximated  
 182 by  $\rho_w \frac{\partial \theta}{\partial t} \equiv \rho_w D_{\theta \psi} \frac{\partial \psi_n}{\partial t} + \rho_w D_{\theta T} \frac{\partial T}{\partial t}$ ; and (v) the total porosity  $\eta$  is assumed to be spatially  
 183 uniform and temporally invariant.

184 **2.2 Functional Parameterizations**185 **2.2.1 Thermophysical Properties of Water, Vapor, and Moist Air**

186 The algorithm for calculating water density,  $\rho_w(T_K)$ , is Equation (2.6) of *Wagner and*  
 187 *Pruess* [2002] and employed only within the temperature range  $273.15 \text{ K} \leq T_K \leq 383.15$   
 188  $\text{K}$  ( $\equiv T_{K, max}$ ). At temperatures greater than  $T_{K, max}$ , then  $\rho_w(T_K) = \rho_w(T_{K, max})$ . This  
 189 approach yields a range for  $\rho_w(T_K)$  of  $950 \text{ kg m}^{-3} < \rho_w(T_K) < 1000 \text{ kg m}^{-3}$ , which represents  
 190 a compromise between the fact that the density of (free saturated liquid) water continues to  
 191 decrease with increasing temperatures [*Yaws* 1995] and the hypothetical possibility that in  
 192 a bound state a mono-layer of liquid water  $\rho_w(T_K)$  may reach values as high as  $\approx 5000 \text{ kg}$   
 193  $\text{m}^{-3}$  [*Danielewicz-Ferchmin and Mickiewicz* 1996].  $d\rho_w/dT$  is computed from the analytical  
 194 expression derived by differentiating the expression for  $\rho_w(T_K)$  and  $d\rho_w/dT = 0$  for  $T_K >$   
 195  $T_{K, max}$ .

196 The enthalpy of vaporization of water,  $H_v = H_v(T_K, \psi)$  [ $\text{J mol}^{-1}$ ], is Equation (5) of

197 *Somayajulu* [1988] augmented by the soil moisture potential,  $\psi$ , [*Massman* 2012; *Campbell*  
 198 *et al.* 1995] and is expressed as follows:

$$H_v = H_1 \left( \frac{T_{crit} - T_K}{T_K} \right) + H_2 \left( \frac{T_{crit} - T_K}{T_{crit}} \right)^{\frac{3}{8}} + H_3 \left( \frac{T_{crit} - T_K}{T_{crit}} \right)^{\frac{9}{4}} - M_w \psi \quad (8)$$

199

200 where  $H_1 = 13.405538 \text{ kJ mol}^{-1}$ ,  $H_2 = 54.188028 \text{ kJ mol}^{-1}$ ,  $H_3 = -58.822461 \text{ kJ mol}^{-1}$ ,  
 201  $T_{crit} = 647.096 \text{ K}$  is the critical temperature for water, and  $M_w = 0.01802 \text{ kg mol}^{-1}$  is the  
 202 molar mass of water vapor. Note that  $h_v = h_v(T_K) [\text{J mol}^{-1}]$  will denote the enthalpy of  
 203 vaporization without the additional  $-M_w \psi$  term, i.e.,  $h_v = h_v(T_K) = H_1 (T_{crit} - T_K) / T_K +$   
 204  $H_2 [(T_{crit} - T_K) / T_{crit}]^{\frac{3}{8}} + H_3 [(T_{crit} - T_K) / T_{crit}]^{\frac{9}{4}}$ . The present formulation differs from *Mass-*  
 205 *man* [2012] because here  $h_v(T_K \geq T_{crit}) = 0$ ; whereas *Massman's* [and *Campbell's et al.* 1995]  
 206 equivalent  $h_v$  was a linear approximation of the present  $h_v$ , which yielded  $h_v(T_K \geq T_{crit}) \gg 0$ .  
 207 This distinction will become important when discussing the water vapor source term,  $S_v$ .  
 208 Note that because  $L_v = H_v / M_w$  it also employs Equation (8).

209 The formulations for thermal conductivity of water vapor,  $\lambda_v = \lambda_v(T_K) [\text{W m}^{-1} \text{ K}^{-1}]$ ,  
 210 and liquid water,  $\lambda_w = \lambda_w(T_K, \rho_w) [\text{W m}^{-1} \text{ K}^{-1}]$ , are taken from *Huber et al.* [2012]. For  
 211 water vapor their Equation (4) is used and for liquid water the product of their Equations  
 212 (4) and (5) is used. The formulations for viscosity of water vapor and liquid water are taken  
 213 from *Huber et al.* [2009] and are similar algorithmically to thermal conductivity. For water  
 214 vapor,  $\mu_v = \mu_v(T_K) [\text{kg m}^{-1} \text{ s}^{-1} \equiv \text{Pa s}]$ , their Equation (11) is used and for liquid water,  
 215  $\mu_w = \mu_w(T_K, \rho_w) [\text{Pa s}]$ , their Equation (36) is used. For liquid water both these formulations  
 216 include a dependence on the density of water. Consequently, once soil temperature exceeds  
 217  $T_{K,max}$  both  $\lambda_w$  and  $\mu_w$  are assigned a fixed value determined at  $T_{K,max}$ . On the other hand,  
 218  $\lambda_v$  and  $\mu_v$  increase continually with increasing temperatures.

219 The formulation for the thermal conductivity of dry air,  $\lambda_d = \lambda_d(T_K) [\text{W m}^{-1} \text{ K}^{-1}]$ , is

220 Equation (5a) of *Kadoya et al.* [1985] and for the viscosity of dry air,  $\mu_d = \mu_d(T_K)$  [Pa  
 221 s], Equation (3a) of *Kadoya et al.* [1985] is used. The model of the thermal conductivity  
 222 of soil atmosphere,  $\lambda_a = \lambda_a(\lambda_v, \lambda_d, \mu_v, \mu_d)$  [W m<sup>-1</sup> K<sup>-1</sup>], is a non-linear expression given  
 223 by Equation (28) of *Tsiliniris* [2008]. The relative weights used in this formulation are  
 224 determined using the mixing ratios for water vapor ( $\chi_v$  [dimensionless]) and dry air ( $\chi_d =$   
 225  $1 - \chi_v$ ): where  $\chi_v = e_v/(P_d + e_v)$ ,  $e_v$  [Pa] is the vapor pressure, and  $P_d$  [Pa] is the dry  
 226 air pressure. Here  $P_d$  will be held constant and equal to the ambient atmospheric pressure,  
 227  $P_{atmos}$  [= 92 kPa], during the laboratory experiments [see *Massman* 2012; *Campbell et al.*  
 228 1995]. The vapor pressure,  $e_v$ , is obtained from  $\rho_v$  and  $T_K$  using the ideal gas law.

229 The volumetric specific heat for soil air,  $\rho_a c_{pa}$  [J m<sup>-3</sup> K<sup>-1</sup>], is estimated for the soil  
 230 atmosphere from  $\rho_a c_{pa} = c_{pv}\rho_v + c_{pd}\rho_d$ ; where  $\rho_d = M_d P_{atmos}/(RT_K)$  [kg m<sup>-3</sup>] is the dry air  
 231 density,  $R = 8.314$  Jmol<sup>-1</sup>K<sup>-1</sup> is the universal gas constant,  $M_d = 0.02896$  kg mol<sup>-1</sup> is the  
 232 molar mass of dry air, and the isobaric specific heats for water vapor,  $c_{pv}$  [J kg<sup>-1</sup> K<sup>-1</sup>], and  
 233 dry air,  $c_{pd}$  [J kg<sup>-1</sup> K<sup>-1</sup>], use Equation (6) of *Bücker et al.* [2003].

234 The saturation vapor pressure,  $e_{v,sat} = e_{v,sat}(T_K)$  [Pa], and its derivative,  $de_{v,sat}/dT$  [Pa  
 235 K<sup>-1</sup>], are modeled using Equations (2.5) and (2.5a) of *Wagner and Pruess* [2002]. The  
 236 saturation vapor density,  $\rho_{v,sat}$  [kg m<sup>-3</sup>], is modeled using Equation (2.7) of *Wagner and*  
 237 *Pruess* [2002]. Following *Massman* [2012], these saturation curves are restricted to temper-  
 238 atures below that temperature,  $T_{K,sat}$ , at which  $e_{v,sat} = P_{atmos}$ . For the present case  $T_{K,sat}$   
 239 = 370.44 K was determined from the saturation temperature equation or “the Backward  
 240 Equation”, Equation (31) of *IAPWS* [2007]. For  $T_K \geq T_{K,sat}$  the saturation quantities  $e_{v,sat}$   
 241 and  $de_{v,sat}/dT$  remain fixed at their values  $T_{K,sat}$ , but  $\rho_{v,sat}$  is allowed to decrease with in-  
 242 creasing temperatures, i.e.,  $\rho_{v,sat} = \rho_{v,sat}(T_{K,sat})[T_{K,sat}/T_K][P_{atmos}/P_{ST}]$ , in accordance with  
 243 Table 13.2 (page 497) of *Wagner and Pruess* [2002], where  $P_{ST} = 101325$  Pa is the standard  
 244 pressure. The present treatment of  $\rho_{v,sat}$  is different from *Massman* [2012], who assumed

245 that  $\rho_{v,sat}(T_K \geq T_{K,sat}) = \rho_{v,sat}(T_{K,sat})$ .

246 Embedded in the hydraulic conductivities [ $K_H$  and  $K_n$  of Equation (2)] are the surface  
 247 tension of water,  $\sigma_w(T_K)$  [ $\text{N m}^{-1}$ ], and the static dielectric constant (or the relative per-  
 248 mittivity) of water,  $\epsilon_w(T_K)$  [*dimensionless*]. These physical properties of water are integral  
 249 to *Zhang's* [2011] model for the hydraulic conductivity associated with film flow, which is  
 250 incorporated into the present model and detailed in a later section. The surface tension of  
 251 water is modeled following Equation (1) of *Vargaftik et al.* [1983] and  $\epsilon_w(T_K)$  is taken from  
 252 Equation (36) of *Fernández et al.* [1997].

### 253 **2.2.2 Functions Related to Water Vapor: $D_{ve}$ , $u_{v1}$ , $S_v$**

254  $D_{ve}$  is modeled as:

$$D_{ve} = \frac{\tau(\eta - \theta)S_F\mathcal{E}D_v}{1 + e_v/P_{atmos}}$$

255 where  $\tau$  [ $\text{m m}^{-1}$ ] is the tortuosity of soil with  $\tau = 0.66[(\eta - \theta)/\eta]^3$  after *Moldrup et al.* [1997],  
 256  $\mathcal{E}$  [*dimensionless*] is the vapor flow enhancement factor and is discussed in *Massman* [2012],  
 257  $D_v/(1 + e_v/P_{atmos})$  [ $\text{m}^2 \text{s}^{-1}$ ] is the molecular diffusivity of water vapor into the soil atmo-  
 258 sphere, which will be taken as a mixture of both dry air and (potentially large amounts of)  
 259 water vapor, and  $S_F$  [*dimensionless*] is Stefan correction or mass flow factor. Externalizing  
 260 the  $1/(1 + e_v/P_{atmos})$  term of the vapor diffusivity and combining it with  $S_F$  allows for the  
 261 following approximation for  $S_F/(1 + e_v/P_{atmos}) = 1/(1 - e_v^2/P_{atmos}^2) \approx 1 + e_v/P_{atmos}$ ; where  
 262 the correct form for  $S_F$  is  $1/(1 - e_v/P_{atmos})$ . The reason for this approximation is to avoid di-  
 263 viding by 0 as  $e_v \rightarrow P_{atmos}$ . *Massman* [2012] and *Campbell et al.* [1995] avoided this issue by  
 264 limiting  $S_F$  to a maximum value of 10/3. This newer approximation for  $S_F/(1 + e_v/P_{atmos})$   
 265 is an improvement over their approach. It is relatively slower to enhance the vapor transport  
 266 by diffusion than the original approach, but this is only of any real significance when  $S_F \geq 1$ .  
 267 On the other hand because the linear form is not limited to any preset maximum value it  
 268 compensates for these underestimations when  $S_F > 10/3$ .

269 Mindful of the externalization of  $1/(1 + e_v/P_{atmos})$ ,  $D_v$  is estimated from the diffusivity  
 270 of water vapor in dry air,  $D_{vd} = D_{vd}(T_K)$  [ $\text{m}^2 \text{s}^{-1}$ ] and the self-diffusivity of water vapor in  
 271 water vapor,  $D_{vv} = D_{vv}(T_K)$  [ $\text{m}^2 \text{s}^{-1}$ ], where

$$D_{vd} = D_{vdST} \left( \frac{P_{ST}}{P_{atmos}} \right) \left( \frac{T_K}{T_{ST}} \right)^{\alpha_{vd}}$$

272 and

$$D_{vv} = D_{vvST} \left( \frac{P_{ST}}{P_{atmos}} \right) \left( \frac{T_K}{T_{ST}} \right)^{\alpha_{vv}}$$

273

274 and  $T_{ST} = 273.15$  K is the standard temperature,  $D_{vdST} = 2.12 \times 10^{-5} \text{ m}^2 \text{ s}^{-1}$ ,  $\alpha_{vd} = 7/4$ ,  
 275  $D_{vvST} = 1.39 \times 10^{-5} \text{ m}^2 \text{ s}^{-1}$ , and  $\alpha_{vv} = 9/4$ . The parameters  $D_{vvST}$  and  $\alpha_{vv}$  relate to the  
 276 self-diffusion of water vapor and their numerical values were determined from a synthesis  
 277 of results from *Hellmann et al.* [2009] and *Yoshida et al.* [2006, 2007]. The uncertainty  
 278 associated with this value for  $D_{vvST}$  is at least  $\pm 15\%$  and possibly more, e.g., *Miles et al.*  
 279 [2012]. Blanc's Law [*Marrero and Mason* 1972] combines  $D_{vd}$  and  $D_{vv}$  to yield the following  
 280 expressions for  $D_v = D_v(T_K, \rho_v)$ :

$$\frac{1}{D_v(T_K, \rho_v)} = \frac{1 - \chi_v}{D_{vd}} + \frac{\chi_v}{D_{vv}} \quad \text{or} \quad D_v(T_K, \rho_v) = \frac{D_{vd}D_{vv}}{(1 - \chi_v)D_{vv} + \chi_v D_{vd}}$$

281

282 The present model for the advective velocity associated with the volatilization of water,  
 283  $u_{vl}$ , is taken from *Ki et al.* [2005] and is non-equilibrium equivalent to that used by *Massman*  
 284 [2012] in his equilibrium model. Here

$$\frac{\partial u_{vl}}{\partial z} = \frac{S_v}{(\eta - \theta)\rho_v} \tag{9}$$

285

286 where the basic assumptions are that both liquid water and vapor are Newtonian fluids and  
 287 that only incompressible effects are being modeled. In essence Equation (9) assumes that the  
 288 vaporization of soil moisture acts as a steady-state (and rapidly expanding or “exploding”)  
 289 volume source term, which yields a 1-D advective velocity associated with volatilization of  
 290 liquid water. For an equilibrium model of soil moisture evaporation that does not include  
 291 water movement (i.e.,  $K_H \equiv 0$ ,  $K_n \equiv 0$ , and  $V_{\theta,surf} \equiv 0$ ), then  $S_v \equiv -\rho_w \partial\theta/\partial t$  (from  
 292 Equation (2) above), which demonstrates the connection between present model of  $u_{vl}$  with  
 293 that used by *Massman’s* [2012]. But unlike *Massman* [2012], the present model does not  
 294 require any numerical adjustments to Equation (9) in order to maintain numerical stability.

295 The functional parameterization of  $S_v$  follows from the non-equilibrium assumption, i.e.,  
 296  $S_v \propto (\rho_{ve} - \rho_v)$ , where  $\rho_{ve} = a_w \rho_{v,sat}(T_K)$  [kg m<sup>-3</sup>] is the equilibrium vapor density and  
 297  $a_w = e^{\frac{M_w \psi^*}{RT_K} \psi_n}$  [*dimensionless*] is the water activity, modeled here with the Kelvin Equation.  
 298 The difficult part is how to construct the proportionality coefficient. Nevertheless, there are  
 299 at least a two ways to go about this: (a) largely empirically [e.g., *Smits et al.* 2011 and  
 300 related approaches referenced therein], or (b) assume that  $S_v = A_{wa} J_v$  [e.g., *Skopp* 1985  
 301 or *Novak* 2012], where  $A_{wa}$  [m<sup>-1</sup>] is the volume-normalized soil water-air interfacial surface  
 302 area and  $J_v$  [kg m<sup>-2</sup> s<sup>-1</sup>] is the flux to/from that interfacial surface. This second approach  
 303 allows a more physically-based parameterization of the flux, viz.,  $J_v = \mathcal{R}_v (\rho_{ve} - \rho_v)$ , where  
 304  $\mathcal{R}_v$  [ms<sup>-1</sup>] is the interfacial surface transfer coefficient. For example, *Novak* [2012] proposed  
 305 that the flux be driven by diffusion, so that  $\mathcal{R}_v = D_v/r_{ep}$ , where  $r_{ep}$  [m] is the equivalent  
 306 pore radius and  $D_v$  is the diffusivity of water vapor in soil air. After a bit of algebra and  
 307 some simple geometrically-based assumptions concerning the relationships between  $r_{ep}$ , a  
 308 spherical pore volume, and  $A_{wa}$ , one arrives at (“the Novak”) model of the source term:

$$S_v^{[M]} = S_*^{[N]} A_{wa}^2 D_v (\rho_{ve} - \rho_v)$$

309

310 where  $S_*^{[N]}$  [*dimensionless*] is an adjustable model parameter.

311 But there is another way to model the vapor flux,  $J_v$ , which is also used in the present  
 312 study. This second approach is based on the Hertz-Knudsen Equation, which has its origins  
 313 in the kinetic theory of gases and describes the net flux of a gas that is simultaneously con-  
 314 densing on and evaporating from a surface. A general expression for the Hertz-Knudsen flux  
 315 is  $J_v = \sqrt{RT_K/M_w} (\mathcal{K}_e \rho_{ve} - \mathcal{K}_c \rho_v)$ , where  $\mathcal{K}_e$  [*dimensionless*] is the mass accommodation (or  
 316 evaporation) coefficient and  $\mathcal{K}_c = \mathcal{K}_c(T_K, \psi_n)$  [*dimensionless*] is the thermal accommodation  
 317 (or condensation) coefficient. For the present purposes  $\mathcal{K}_e \equiv 1$  can be assumed. This model  
 318 of  $J_v$  yields the following model for  $S_v$ :

$$S_v^{[M]} = S_*^{[M]} A_{wa} \sqrt{\frac{RT_K}{M_w}} (\rho_{ve} - \mathcal{K}_c \rho_v) \quad (10)$$

319

320 where  $S_*^{[M]}$  [*dimensionless*] is an adjustable model parameter, to be determined by “tuning”  
 321 it as necessary to ensure model stability. This model for  $S_v^{[M]}$  is now more or less complete,  
 322 but the model for  $S_v^{[N]}$  is neither quite complete nor precisely comparable to  $S_v^{[M]}$ . This is  
 323 now remedied by introducing  $\mathcal{K}_c$  into  $S_v^{[N]}$  and subsuming a factor of  $A_{wa}$  into  $S_*^{[N]}$ , yielding:

$$S_v^{[N]} = S_*^{[N]} A_{wa} D_v (\rho_{ve} - \mathcal{K}_c \rho_v) \quad (11)$$

324

325 where  $S_*^{[N]}$  [ $\text{m}^{-1}$ ] now has physical dimensions, but otherwise remains an adjustable param-  
 326 eter that will be scaled such that  $S_v^{[N]} \approx O(S_v^{[M]})$ . In this form these two models for  $S_v$



327 can be used to test the sensitivity of the model's solution to different temperature forcing,  
 328 because  $S_v^{[M]} \propto \sqrt{T_K}$ , whereas  $S_v^{[N]} \propto T_K^\alpha$ , where  $\alpha \geq 2$ .

329 Concluding the development of  $S_v$  requires models of  $\mathcal{K}_c$  and  $A_{wa} = A_{wa}(\theta)$ .  $\mathcal{K}_c$  is  
 330 parameterized as

$$\mathcal{K}_c(T_K, \psi_n) = e^{\frac{E_{av} - M_w \psi}{R} \left( \frac{1}{T_K} - \frac{1}{T_{K,in}} \right)}$$

331

332 where  $T_{K,in}$  [K] is the initial temperature of the laboratory experiments and because  $T_K \geq$   
 333  $T_{K,in}$  throughout the experiment  $\mathcal{K}_c \leq 1$  throughout the experiment and  $E_{av} - M_w \psi$  [J mol<sup>-1</sup>]  
 334 is an empirically determined surface condensation/evaporation activation energy. (Note: the  
 335 enthalpy of vaporization,  $h_v(T_K)$ , is a logical choice for  $E_{av}$ . Nevertheless, model perfor-  
 336 mance was significantly enhanced by simply assigning a constant value for  $E_{av} \approx 30 - 40$  kJ  
 337 mol<sup>-1</sup> rather than using  $h_v$ .) The present formulation ensures that  $\partial \mathcal{K}_c / \partial T_K < 0$ , in accor-  
 338 dance with experimental and theoretical studies [Tsuruta and Nagayama 2004; Kon et al.  
 339 2014]. Mathematically this present formulation of  $\mathcal{K}_c$  largely eliminates model instabilities  
 340 by suppressing condensation relative to evaporation throughout the experiment and will be  
 341 discussed in greater detail in a later section.

342  $A_{wa}$  is parameterized as a parabolic function to simulate the conceptual model of  $A_{wa}$   
 343 proposed by *Constanza-Robinson and Brusseau* [2002: see their Figure (1b)]:

$$A_{wa}(\theta) = \mathcal{S}_w(1 - \mathcal{S}_w)^{a_1} + a_2[\mathcal{S}_w(1 - \mathcal{S}_w)]^{a_3}$$

344

345 where  $\mathcal{S}_w = \theta/\eta$  is the soil water saturation and  $a_1 = 40$ ,  $a_2 = 0.003$ , and  $a_3 = 1/8$ . This  
 346 particular functional form ensures that  $A_{wa} = 0$  when the soil is completely dry,  $\theta = 0$ , and  
 347 when fully saturated,  $\mathcal{S}_w = 1$ . This particular parameter value for  $a_1$  was chosen so that

348 the maximum value of  $A_{wa}$  occurs at  $\mathcal{S}_w = 0.025$  ( $=1/a_1$ ) in accordance with the model of  
 349 *Constanza-Robinson and Brusseau* [2002].

### 350 **2.2.3 Thermal Transport Properties: $C_s$ , $\lambda_s$**

351 The model for  $C_s(T, \theta)$  is taken from *Massman* [2012]:  $C_s(\theta, T) = c_s(T)\rho_b + C_w(T)\theta$ ,  
 352 where  $\rho_b$  [ $\text{kg m}^{-3}$ ] is the soil bulk density;  $c_s(T) = c_{s0} + c_{s1}T$  [ $\text{J kg}^{-1} \text{K}^{-1}$ ] is the specific heat  
 353 capacity of soil; and  $C_w(T) = C_{w0} + C_{w1}T + C_{w2}T^2$  [ $\text{J m}^{-3} \text{K}^{-1}$ ] is the volumetric heat capacity  
 354 of water; and the parameterization constants  $c_{s0}, c_{s1}, C_{w0}, C_{w1}, C_{w2}$  are given by *Massman*  
 355 [2012]. Note that the present  $C_s(\theta, T)$  results from approximating  $C_w(T) \equiv c_{pw}(T)\rho_w(T_K)$   
 356 by  $c_{pw}(T)\rho_w(T_{ST})$ , where  $c_{pw}(T)$  [ $\text{J kg}^{-1} \text{K}^{-1}$ ] is the isobaric specific heat capacity of water,  
 357 and  $\rho_w(T_{ST}) = 1000 \text{ kg m}^{-3}$ . This substitution for  $\rho_w(T_K)$  is only made for  $C_w(T)$ .

358 The present formulation for isobaric heat capacity of water,  $c_{pw}(T)$ , was developed from  
 359 *Yaws* [1995] and confirmed by comparing to *Wagner and Pruess* [2002]. In general  $c_{pw}(T)$   
 360 is also a function of pressure [*e.g.*, *Wagner and Pruess* 2002], but this dependency can  
 361 be ignored for the present purposes. Other parameterization of  $c_{pw}(T)$  [*i.e.*, *Sato* 1990;  
 362 *Jovanović et al.* 2009; *Kozłowski* 2012] were also examined, but proved unsatisfactory.  
 363 Finally, *Kozłowski* [2012] reports numerical values for the dry soil parameters  $c_{s0}$  and  $c_{s1}$   
 364 that are similar to those discussed in *Massman* [2012] and used with the present model.

365 The model of soil thermal conductivity,  $\lambda_s$ , is the sum of two terms. The first,  $\lambda_s^{[1]}(\theta, T_K, \rho_v)$ ,  
 366 is taken principally from *Campbell et al.* [1994] and the second,  $\lambda_s^{[2]}(\theta, T_K)$ , is taken from  
 367 *Bauer* [1993]. This second term incorporates the effects of high-temperature thermal (in-  
 368 frared) radiant energy transfer within the soil pore space, which may be significant for certain  
 369 soils and high enough temperatures [*e.g.*, *Durany et al.* 2010].  $\lambda_s^{[1]}$  is summarized first and  
 370 repeated here to emphasize the difference between the present model's functional parame-  
 371 terizations and those used in *Massman* [2012].

372  $\lambda_s^{[1]}$  is modeled as:

$$\lambda_s^{[1]}(\theta, T_K, \rho_v) = \frac{k_w \theta \lambda_w(T_K, \rho_w) + k_a [\eta - \theta] \lambda_a^*(\theta, T_K, \rho_v) + k_m [1 - \eta] \lambda_m}{k_w \theta + k_a [\eta - \theta] + k_m [1 - \eta]} \quad (12)$$

373

374 where  $\lambda_a^*(\theta, T_K, \rho_v) = \lambda_a(T_K) + \lambda_v^*(\theta, T_K, \rho_v)$  is the apparent thermal conductivity of the soil  
 375 air and is the sum of the thermal conductivity of moist soil air,  $\lambda_a$ , and  $\lambda_v^*$ , which incorporates  
 376 the effects of latent heat transfer;  $\lambda_m$  is the thermal conductivity of the mineral component  
 377 of the soil, which is assumed to be independent of temperature and soil moisture; and  $k_w$ ,  
 378  $k_a$ , and  $k_m$  [*dimensionless*] are generalized formulations of the de Vries weighting factors  
 379 [*de Vries* 1963]. *Campbell et al.* [1994] formulate  $\lambda_v^*$  as proportional to the product of the  
 380 enthalpy of vaporization ( $h_v$ ), the vapor diffusivity ( $D_v$ ), the Stefan factor ( $S_F$ ), the slope  
 381 of the saturation vapor pressure ( $de_{v,sat}/dT$ ), and the parameter  $f_w(\theta, T)$  (*Campbell et al.*  
 382 [1995] also used in the diffusivity enhancement factor,  $\mathcal{E}$ ). For present model  $\lambda_v^*$  is

$$\lambda_v^*(\theta, T_K, \rho_v) = \frac{\hat{\rho}_{ST} h_v f_w S_F D_v [de_{v,sat}/dT]}{P_{atmos}} \quad (13)$$

383

384 where  $\hat{\rho}_{ST} = 44.65 \text{ mol m}^{-3}$  is the molar density of the standard atmosphere. Equations (12)  
 385 and (13) are the same as those used in *Massman* [2012], but numerically they yield quite  
 386 results due to the different formulations for  $h_v$ ,  $S_F$ ,  $D_v$ , and  $e_{v,sat} = e_{v,sat}(T_K)$ . Otherwise  
 387 the *de Vries* [1963] shape factors, the parameter  $f_w$ , and all related parameters are the same  
 388 as in *Massman* [2012].

389  $\lambda_s^{[2]}$  is modeled as:

$$\lambda_s^{[2]}(\theta, T_K) = 3.8 \sigma N^2 R_p T_K^3 \quad (14)$$

390

391 where  $\sigma = 5.670 \times 10^8 \text{ W m}^{-2} \text{ K}^{-4}$  is the Boltzmann constant;  $N = N(\theta) = 1 + \theta/(3\eta)$  is  
392 the medium's [*dimensionless*] index of refraction;  $R_p$  [m] is the soil's pore space volumetric  
393 radius; and the factor of 3.8 subsumes a numerical factor of 4, a [*dimensionless*] pore shape  
394 factor (= 1 for spherical particles), and the [*dimensionless*] emissivity of the medium  $\approx 0.95$   
395 (by assumption). In general  $R_p$  is considered to be a model parameter and it will be varied  
396 to evaluate the model's sensitivity and performance relative to  $\lambda_s^{[2]}$ . But unless otherwise  
397 indicated,  $R_p = 10^{-3}$  m is the nominal or default value.

### 398 2.2.4 Water Retention Curve

399 In general a WRC is a functional relationship between soil moisture and soil moisture  
400 potential and temperature, i.e.,  $\theta = \theta(\psi, T)$ , although the temperature dependency is often  
401 ignored and was of little consequence to *Massman's* [2012] model. The three WRCs tested  
402 in the present study have been adapted to include a residual soil moisture,  $\theta_r = \theta_r(\psi, T)$   
403 [ $\text{m}^3\text{m}^{-3}$ ], which is an atypical parameterization for both  $\theta_r$  and the soil moisture's temper-  
404 ature dependency. Under more normal soil environmental conditions  $\theta_r$  is assumed to be  
405 bound so securely to soil mineral surfaces that it is normally taken as a fixed constant. For  
406 the present purposes the principal WRC is adapted from *Massman* [2012] and is

$$\theta(\psi_n, T_K) = -\frac{\theta_l}{\alpha_l} \ln(\psi_n) + \left[ \theta_h - \theta_r(\psi_n, T_K) \right] \left[ 1 + (\alpha_h \psi_n)^4 \right]^{-\frac{1}{p}} + \theta_r(\psi_n, T_K) \quad (15)$$

407

408 Where

$$\theta_r(\psi_n, T_K) = \theta_{r*} e^{\frac{b_1 E_{av}(1-b_2 \psi_n)}{R} \left( \frac{1}{T_K} - \frac{1}{T_{K,in}} \right)} \quad (16)$$

409

410 and  $\theta_l$  [ $\text{m}^3 \text{m}^{-3}$ ] is the extrapolated value of the water content when  $\psi = \psi_l = -1 \text{ J kg}^{-1}$ ;  
411  $\alpha_l = \ln(\psi_*/\psi_l) = 13.8155106$ ; and  $\theta_h$  [ $\text{m}^3 \text{m}^{-3}$ ],  $\alpha_h$  [*dimensionless*] and  $p$  [*dimensionless*]

412 are parameters obtained from *Campbell and Shiozawa* [1992],  $\theta_{r*}$  [ $\text{m}^3 \text{m}^{-3}$ ] is a constant  
 413 soil-specific parameter, such that  $\theta_{r*} \leq 0.03$  is to be expected, and  $b_1$  [*dimensionless*] and  
 414  $b_2$  [*dimensionless*] are adjustable parameters, which are expected to satisfy  $b_1 > 0$  and  
 415  $0 \leq b_2 < 1$ . Note: further discussion concerning the original version of Equation (15) can be  
 416 found in *Massman* [2012].

417 There is a simple and physically intuitive argument for this particular parameterization  
 418 of  $\theta_r(\psi_n, T_K)$  in Equation (16). First, under more normal soil environmental conditions, i.e.,  
 419  $T_K \approx T_{K,in}$  and at least  $\psi_n < 1$  (if not  $\psi_n \ll 1$ ), then it is reasonable to expect that  $\theta_r \approx \theta_{r*}$   
 420 and nearly constant throughout (what might be expected to be relatively small variations  
 421 in) those conditions. But as the temperature increases, it is also reasonable to assume that  
 422 the increasing amounts of thermal energy will begin to overcome the forces holding the  
 423 bound water to the soil mineral surfaces and that  $\theta_r$  will decrease. Mathematically, then one  
 424 might therefore expect that  $\partial\theta_r/\partial T_K < 0$ . *Massman* [2012: see his discussion of  $\psi_T$ ] made  
 425 similar arguments when he included the temperature dependency in his version of the same  
 426 basic WRC. Consequently, the Equations (15) and (16) above offer a different approach  
 427 to including temperature effects on the WRC that maintains the temperature dependent  
 428 properties of WRCs outlined by *Massman* [2012]. Second, as the temperature increases  
 429 and the soil moisture (including  $\theta_r$ ) begins to decrease, the soil moisture potential  $\psi_n$  will  
 430 begin to increase (or  $\psi < 0$  will decrease in absolute terms while increasing in magnitude),  
 431 which in turn (it is hypothesized) will tend to strengthen the forces holding the bound water.  
 432 Therefore, one might expect that as the soil dries out  $\partial\theta_r/\partial\psi_n > 0$ , which will oppose, but  
 433 not dominate the temperature effects, i.e.,  $b_2 < 1$ . Equation (16) is designed to capture these  
 434 two opposing influences, assuming of course that  $T_K > T_{K,in}$ . But, it is itself not intended to  
 435 be a fully physically-based dynamical theory of the residual soil moisture. Such a theory is  
 436 beyond the intent of the present study. The sole intent here is to test and evaluate whether a

437 dynamical  $\theta_r$  can improve the model's performance. And in so far as it may succeed at doing  
 438 so, it will also indicate the value and need for a more detailed physically-based dynamical  
 439 model of  $\theta_r$ .

440 The present study also includes similar adaptations to two other WRCs so as to test  
 441 the model's sensitivity to different WRCs. These WRCs, which will not be shown here, are  
 442 taken from *Groenevelt and Grant* [2004] and *Fredlund and Xing* [1994].

### 443 2.2.5 Functions Related to Liquid Water Transport: $\mathbf{K}_n$ , $\mathbf{K}_H$ , $\mathbf{V}_{\theta, \text{surf}}$

444 The hydraulic conductivity functions,  $K_n(T_K, \psi_n, \theta)$  and  $K_H(T_K, \psi_n, \theta)$ , are given as fol-  
 445 lows:

$$K_n = \frac{K_I K_R \rho_w}{\mu_w} \psi_* \quad \text{and} \quad K_H = \frac{K_I K_R \rho_w}{\mu_w} g$$

446

447 where  $g = 9.81 \text{ m s}^{-2}$  is the acceleration due to gravity;  $K_I [\text{m}^2]$  is the intrinsic permeability  
 448 of the soil (a constant for any given soil); and  $K_R = K_R(\theta, \theta_r, \psi_n, T_K)$  [*dimensionless*] is  
 449 the hydraulic conductivity function (HCF), which for the present study is taken as the sum  
 450 of  $K_R^{cap}$  (associated with capillary flow) and  $K_R^{film}$  (associated with film flow). The model  
 451 for intrinsic permeability, which is taken from *Bear* [1972], is  $K_I = (6.17 \times 10^{-4}) d_g^2$ ; where  
 452  $d_g$  [m] is the mean or 'effective' soil particle diameter. For the soils used in the present  
 453 work [*Campbell et al.* 1995; *Massman* 2012]  $d_g$  was estimated from *Shiozawa and Campbell*  
 454 [1991] and *Campbell and Shiozawa* [1992] or simply assigned a reasonable value if no other  
 455 information was available.

456 For present study five difference parameterizations for  $K_R^{cap}$  were tested. Two were from  
 457 *Grant et al.* [2010], i.e., their Equation (18) [Burdine] and Equation (19) [Mualem]; the *Van*  
 458 *Genuchten and Nielson* [1985] model, their Equation(22) with the mathematical constraints  
 459 imposed as suggested by *Assouline and Or* [2013]; the *Brooks and Corey* [1964] model; and

460 Equation (18) of *Assouline* [2001]. The reason for testing several models of the HCF is to  
 461 determine how different formulations for the HCF might impact the model's performance  
 462 when comparing to the laboratory observations. The following HCF is *Assouline's* [2001]  
 463 model, which is a relatively simple formulation for the HCF and serves as the reference HCF  
 464 for the model simulations.

$$K_R^{cap}(\theta, \theta_r) = \left( 1 - \left[ 1 - \left( \frac{\theta - \theta_r(\psi_n, T_K)}{\eta} \right)^{\frac{1}{m}} \right]^m \right)^n \quad (17)$$

465

466 where for the present application  $0 < m < 1$ , and  $n > 1$ .

467  $K_R^{film}(T_K, \psi_n)$  is taken from *Zhang* [2011] and is expressed, in the present notation, as:

$$K_R^{film}(T_K, \psi_n) = \frac{\mathcal{R}_w(T_K)}{6.17 \times 10^{-4}} \left[ \frac{2\sigma_w}{2\sigma_w - \rho_w d_g \psi_* \psi_n} \right]^{\frac{3}{2}} \quad (18)$$

468

469 and

$$\mathcal{R}_w(T_K) = \sqrt{2} \pi^2 (1 - \eta) \mathcal{F}_w \left[ \left( \frac{\epsilon_0 \epsilon_w}{2\sigma_w d_g} \right)^{\frac{1}{2}} \left( \frac{k_B T_K}{z a} \right) \right]^3 \quad (19)$$

470

471 where (as above)  $\sigma_w(T_K)$  is the surface tension of water and  $\epsilon_w(T_K)$  is the static dielectric  
 472 constant or relative permittivity of water;  $\epsilon_0 = 8.85 \times 10^{-12} \text{ C}^2 \text{ J}^{-1} \text{ m}^{-1}$  is the permittivity of  
 473 free space;  $k_B = 1.308568 \times 10^{-23} \text{ J K}^{-1}$  is the Boltzmann constant;  $a = 1.6021773 \times 10^{-19} \text{ C}$  is  
 474 the electron charge;  $z$  [*dimensionless*] is the ion charge, for which  $z = 1$  can be assumed; and  
 475  $\mathcal{F}_w$  [*dimensionless*] is a soil-specific parameter, for which *Zhang* [2011] found that (roughly)  
 476  $10 < \mathcal{F}_w < 10^4$ .

477 The term  $\rho_w V_{\theta, surf}$  in Equation (2) represents the soil moisture movement caused by water  
 478 molecules “hopping” or “skipping” along the surface of the water films due to a temperature  
 479 gradient [e.g., *Medveď and Černý* 2011]. The present model for  $V_{\theta, surf}$  is adapted from the  
 480 model of *Gawin et al.* [1999] and is given as:

$$V_{\theta, surf} = -D_{\theta s} \frac{\partial \theta}{\partial z} = -D_{\theta s} D_{\theta \psi} \frac{\partial \psi_n}{\partial z} - D_{\theta s} D_{\theta T} \frac{\partial T}{\partial z} \quad (20)$$

481

482 where  $D_{\theta s} = D_{\theta s}(T_K, \theta)$  [ $\text{m}^2\text{s}^{-1}$ ] is the surface diffusivity and is parameterized as:

$$D_{\theta s} = D_{\theta s0} \exp \left[ -2 \left( \frac{\theta}{\theta_b} \right)^\beta \left( \frac{T_{ST}}{T_K} \right) \right] \quad (21)$$

483

484 with  $D_{\theta s0} \approx 10^{-10} \text{ m}^2\text{s}^{-1}$ ;  $\theta_b \approx 0.02$ ; and  $\beta = 1/4$  when  $\theta \geq \theta_b$  or otherwise  $\beta = 1$  when  
 485  $\theta < \theta_b$ .

486 By expressing  $V_{\theta, surf}$  in terms of the gradient of the “normalized” soil moisture potential,  
 487  $\psi_n$ , in Equation (20),  $K_n^*$  and  $K_m$ , used in Equations (5) and (6), can be identified as:  
 488  $K_n^* = K_n + D_{\theta s} D_{\theta \psi}$  and  $K_m = D_{\theta s} D_{\theta T}$ ; where  $D_{\theta s} D_{\theta \psi}$  will be defined as  $K_n^{surf}$ ; where  
 489  $K_n^{surf} \leq 0 \forall T_K$  and  $\theta$ .

### 490 3. Numerical Implementation

491 The numerical model as outlined above and detailed in this section is coded as MATLAB  
 492 (The MathWorks Inc., Natick, MA, Version R2013b) script files.

#### 493 3.1 Crank-Nicolson Method

494 The linearized Crank-Nicolson method is used to solve Equations (5), (6), and (7). For  
 495 Equation (5) this yields the following (canonical) linear finite difference equation:

$$-A_{TTi}^j T_{i-1}^{j+1} + [1 + B_{TTi}^j] T_i^{j+1} - C_{TTi}^j T_{i+1}^{j+1} + A_{T\psi i}^j \psi_{ni-1}^{j+1} - [\Gamma_{T\psi i}^j - B_{T\psi i}^j] \psi_{ni}^{j+1} + C_{T\psi i}^j \psi_{ni+1}^{j+1} =$$



$$A_{TTi}^j T_{i-1}^j + [1 - B_{TTi}^j] T_i^j + C_{TTi}^j T_{i+1}^j - A_{T\psi i}^j \psi_{ni-1}^j - [\Gamma_{T\psi i}^j + B_{T\psi i}^j] \psi_{ni}^j - C_{T\psi i}^j \psi_{ni+1}^j \quad (22)$$

where  $j$  and  $j + 1$  are consecutive time indices,  $i - 1$ ,  $i$ , and  $i + 1$  are contiguous spatial indices, and  $A_{TTi}^j$ ,  $B_{TTi}^j$ ,  $C_{TTi}^j$ ,  $A_{T\psi i}^j$ ,  $B_{T\psi i}^j$ ,  $C_{T\psi i}^j$ , and  $\Gamma_{T\psi i}^j$  are the linearized C-N coefficients, which will not be explicitly listed here, but they do largely follow conventions and notation similar to *Massman* [2012]. Although containing more terms than Equation (22), the finite difference equation corresponding to Equation (6) is very similar. But to linearize Equation (7), the Crank-Nicolson scheme requires linearizing the source term,  $S_v(T, \theta, \psi, \rho_v)$ . This is done with a first order Taylor series expansion of the C-N term  $S_v^{j+1}$  as follows:

$$S_{vi}^{j+1} = S_{vi}^j + \left( \frac{\delta S_v}{\delta T} \right)_i^j (T_i^{j+1} - T_i^j) + \left( \frac{\delta S_v}{\delta \psi_n} \right)_i^j (\psi_{ni}^{j+1} - \psi_{ni}^j) + \left( \frac{\partial S_v}{\partial \rho_v} \right)_i^j (\rho_{vi}^{j+1} - \rho_{vi}^j)$$

where  $\frac{\delta S_v}{\delta T} = D_{\theta T} \frac{\partial S_v}{\partial \theta} + \frac{\partial S_v}{\partial T}$  and  $\frac{\delta S_v}{\delta \psi_n} = D_{\theta \psi} \frac{\partial S_v}{\partial \theta} + \frac{\partial S_v}{\partial \psi_n}$ , which in turn yields the following linearized finite difference equation for Equation (7):

$$\begin{aligned} & - \left[ \frac{\Delta t}{2(\eta - \theta)_i^j} \left( \frac{\delta S_v}{\delta T} \right)_i^j \right] T_i^{j+1} - \left[ B_{\rho \psi i}^j + \frac{\Delta t}{2(\eta - \theta)_i^j} \left( \frac{\delta S_v}{\delta \psi_n} \right)_i^j \right] \psi_{ni}^{j+1} \\ & - A_{\rho \rho i}^j \rho_{vi-1}^{j+1} + \left[ 1 + B_{\rho \rho i}^j - \frac{\Delta t}{2(\eta - \theta)_i^j} \left( \frac{\partial S_v}{\partial \rho_v} \right)_i^j \right] \rho_{vi}^{j+1} - C_{\rho \rho i}^j \rho_{vi+1}^{j+1} = \\ & - \left[ \frac{\Delta t}{2(\eta - \theta)_i^j} \left( \frac{\delta S_v}{\delta T} \right)_i^j \right] T_i^j - \left[ B_{\rho \psi i}^j + \frac{\Delta t}{2(\eta - \theta)_i^j} \left( \frac{\delta S_v}{\delta \psi_n} \right)_i^j \right] \psi_{ni}^j \end{aligned}$$

$$+A_{\rho\rho i}^j \rho_{vi-1}^j + \left[ 1 - B_{\rho\rho i}^j - \frac{\Delta t}{2(\eta - \theta)_i^j} \left( \frac{\partial S_v}{\partial \rho_v} \right)_i^j \right] \rho_{vi}^j + C_{\rho\rho i}^j \rho_{vi+1}^j + \frac{\Delta t}{(\eta - \theta)_i^j} S_{vi}^j \quad (23)$$

509

510 where  $B_{\rho\psi i}^j$ ,  $A_{\rho\rho i}^j$ ,  $B_{\rho\rho i}^j$ , and  $C_{\rho\rho i}^j$  are linearized C-N coefficients related to the transport terms  
 511 of Equation (7) and  $\Delta t$  [s] is the time step. Here  $\Delta t = 1.2$  s and was chosen after testing  
 512 the model at  $\Delta t = 0.3$  s and  $\Delta t = 0.6$  s to ensure no degradation in model performance or  
 513 solution stability at the larger time step.

### 514 3.2 Upper Boundary Conditions

515 The upper boundary condition on heat and vapor transfer are formulated in terms of the  
 516 surface energy balance and, except for the latent heat flux, is identical to *Massman's* [2012]  
 517 upper boundary condition.

$$\epsilon(\theta_0) Q_R^\downarrow(t) = \epsilon(\theta_0) \sigma T_{K0}^4 + \rho_a c_{pa} C_H [T_0 - T_{amb}(t)] + L_{v0} E_0 + G_0 \quad (24)$$

518 where the '0' subscript refers to the surface and the terms from left to right are: the incoming  
 519 or down welling radiant energy,  $Q_R^\downarrow(t)$  [ $\text{W m}^{-2}$ ], absorbed by the surface, which is partitioned  
 520 into the four terms (fluxes) on the right side of the equation, the infrared radiation lost by  
 521 the surface, the surface sensible or convective heat, the surface latent heat, and the surface  
 522 soil heat flux.  $Q_R^\downarrow(t)$  and  $T_{amb}(t)$  are functions of time and are prescribed externally as  
 523 discussed in *Massman* [2012]. The soil surface emissivity,  $\epsilon(\theta_0)$  [*dimensionless*], is a function  
 524 of soil moisture and is taken from *Massman* [2012], as is surface heat transfer coefficient  $C_H$   
 525 [ $\text{m s}^{-1}$ ]; and  $\sigma$  is the Stefan-Boltzmann constant.

526 The surface evaporation rate,  $E_0$  [ $\text{kg m}^{-2} \text{s}^{-1}$ ], is parameterized as

$$E_0 = h_{s0} C_E [\rho_{v0} - \rho_{v\text{amb}}(t)] \quad (25)$$

527

528 where  $h_{s0} \equiv a_{w0} = \exp([M_w \psi_* \psi_{n0}] / [RT_{K0}])$  [*dimensionless*] is the ‘surface humidity’, here  
529 modeled as the water activity at the surface using the Kelvin Equation;  $C_E$  [ $\text{m s}^{-1}$ ] is the  
530 surface the transfer coefficient, an adjustable model parameter but one that can reason-  
531 ably be assumed to be between about  $10^{-4} \text{ m s}^{-1}$  [*Jacobs and Verhoef 1997*] and  $10^{-3} \text{ m}$   
532  $\text{s}^{-1}$  [*Massman 2012*]. Finally, in the case of the laboratory experiments of *Campbell et al.*  
533 [1995],  $\rho_{v\text{amb}}(t)$ , like  $T_{\text{amb}}(t)$  and  $Q_R^\downarrow(t)$ , is an external forcing function at the soil surface.  
534 The present formulation of  $E_0$  results from combining and adapting the expressions for the  
535 potential evaporation rate for soils developed by *Jacobs and Verhoef [1997]* and Equation  
536 (9.14) of *Campbell [1985]*. For this formulation the surface relative humidity,  $h_{s0}$ , is the sur-  
537 face property that constrains or reduces the surface evaporation  $E_0$  to less than the potential  
538 rate.

539 The upper boundary condition on soil water is  $(\partial\theta/\partial z)_0 = 0$ , which when employed with  
540 the WRC, Equation (15), yields the following upper boundary condition on the conservation  
541 of soil moisture, Equation (6):

$$\left(\frac{\partial\psi_n}{\partial z}\right)_0 = \left(\frac{D_{\theta T}}{D_{\theta\psi}}\right)_0 \frac{G_0}{\lambda_{s0}} \quad (26)$$

542

543 The boundary forcing functions  $e_{v\text{amb}}(t)$  [Pa] (the ambient vapor pressure),  $T_{\text{amb}}(t)$ , and  
544  $Q_R^\downarrow(t)$  are taken from *Massman [2012]*, which in turn were adapted to the laboratory data  
545 of *Campbell et al. [1995]*. They take the following generic form:

$$V(t) = V_i e^{-t/\tau} + V_f (1 - e^{-t/\tau})$$

546 where  $V_i$  is the value of the function at the beginning of the soil heating experiment,  $V_f$  is the  
547 value of the function at the end of the experiment, and  $\tau$  [s] is a time constant of the heating  
548 source, which varies with each individual soil heating experiment.  $\rho_{v\text{amb}}(t)$  is obtained from

549  $e_{v\text{amb}}(t)$  and  $T_{\text{amb}}(t)$  using the ideal gas law.

### 550 **3.3 Lower Boundary Conditions and Initial Conditions**

551 As with the companion model [Massman 2012], a numerical (or extrapolative or “pass-  
552 through”) lower boundary condition [Thomas 1995] is also used for the present model. An-  
553 alytically this is equivalent to assuming that the second spatial derivative ( $\partial^2/\partial z^2$ ) of all  
554 model variables is zero at the lower boundary. It is used here for the same reason as with  
555 the previous model: principally for convenience because it is likely to be nearly impossible to  
556 specify any other the lower boundary condition during a real fire. The boundary condition  
557 on the advective velocity is  $u_{vt} = 0$  at the bottom boundary, which is also the same as  
558 with Massman [2012] and Campbell *et al.* [1995]. Further discussion on the model’s lower  
559 boundary conditions can be found in Massman [2012].

560 Except for the initial value of  $\psi_{in}$  (or  $\psi_{n,in}$ ), all initial conditions (soil temperature and  
561 moisture content), which are assumed to be uniform throughout the soil column for each  
562 soil type and heating experiment, are taken directly from Campbell *et al.* [1995]. The initial  
563 value for  $\psi$  is obtained by inverting (solving for it using) the WRC after inputting the initial  
564 values for soil temperature and moisture content. Consequently,  $\psi_{n,in}$  can vary with the  
565 specific WRC.

## 566 **4. Results**

### 567 **4.1 Recalibration of Observed Volumetric Soil Moisture**

568 In the original soil heating experiments of Campbell *et al.* [1995] soil temperatures were  
569 measured with copper-constantan thermocouples at the sample surface and at 5, 15, 25, 35,  
570 65, and 95 mm depth and changes in soil moisture were obtained by gamma ray attenua-  
571 tion at the same depths (except the surface). The moisture detecting system was linearly  
572 calibrated for each experimental run between (a) the initial soil moisture amounts, which  
573 were determined gravimetrically beforehand, and (b) the point at which the sample was

574 oven-dried (also determined before the heating experiment) where  $\theta = 0$  is assumed. But  
575 oven-drying a soil will not necessarily remove all the liquid water from a soil, i.e., a soil  
576 can display residual water content,  $\theta_r$ , after oven-drying. Consequently, the soil moisture  
577 data obtained and reported by *Campbell et al.* [1995] show negative soil moistures at the  
578 time the soil dryness passes outside the oven-dry range. *Massman* [2012] commented on this  
579 issue. With the present study, all volumetric soil moisture data were first adjusted (using a  
580 linear transformation) to rescale the observed soil moisture,  $\theta_{observed}$ , so that the values of  
581  $\theta_{observed} < 0$  became  $\theta_{observed} \approx 0$ . This re-scaling had very little impact on any values of  
582  $\theta_{observed}$  except those asymptotic data where  $\theta_{observed} < 0$ . Furthermore, this re-calibration  
583 is reasonable so long as the original calibration was linear and based on a Beer's Law type  
584 extinction coefficient (which would be linearly related to the logarithm of the attenuation of  
585 gamma ray intensity).

## 586 4.2 Model Performance

587 The present model is evaluated against five of *Campbell et al.*'s [1995] soil heating exper-  
588 iments: (1) Quincy Sand, which has an initial soil moisture content =  $\theta_{in} = 0.14 \text{ m}^3 \text{ m}^{-3}$ ;  
589 (2) Dry Quincy Sand with  $\theta_{in} = 0.03 \text{ m}^3 \text{ m}^{-3}$ , (3) Dry Palouisse B with  $\theta_{in} = 0.07 \text{ m}^3 \text{ m}^{-3}$ ,  
590 (4) Wet Palouisse B with  $\theta_{in} = 0.17 \text{ m}^3 \text{ m}^{-3}$ , and (5) Wet Boulder creek with  $\theta_{in} = 0.22 \text{ m}^3$   
591  $\text{m}^{-3}$ . But here the focus is principally on Quincy Sand and Wet Palouisse B. Most of the  
592 major conclusions regarding the present model can be drawn from these two experiments and  
593 including Quincy Sand here also benefits comparisons with *Massman* [2012], who also tested  
594 his equilibrium model against the Quincy Sand data. But in addition to a general assessment  
595 of model performance, these two experiments also serve as vehicles for a sensitivity analysis  
596 of the key physical processes and parameterizations discussed in the previous two sections.  
597 Thus, the Quincy Sand experiment is also used to explore the importance of the infrared  
598 component of the soil thermal conductivity [ $\lambda_s^{[2]}$ : Equation (14)] and the Wet Palouisse B

599 experiment is also used to evaluate the potential contribution of the dynamic residual soil  
600 moisture  $[\theta_r(\psi_n, T_K)$ : Equations (15), (16) and (17)] to the model’s performance. Finally,  
601 because the HCF [Equation (17)], is central to the overall performance of the model it is  
602 discussed in more detail a separate section following the Quincy Sand results.

#### 603 4.2.1 Quincy Sand

604 Figure 1 compares the measured (symbols) and modeled (lines) of soil temperature dur-  
605 ing the Quincy Sand heating experiment for two model runs with different values of  $R_p$ .  
606 Increasing  $R_p$  to 4 mm (dashed lines) over the default value of 1 mm (solid lines) increases  
607 the infrared component of the soil thermal conductivity,  $\lambda_s^{[2]}$ . Because the model’s perfor-  
608 mance was not enhanced by the inclusion of either the residual soil moisture,  $\theta_r$ , or film flow,  
609  $K_R^{film}$ , neither are included as part of the Quincy sand simulations. The colors indicate the  
610 depths (mm) of the experimental and model data. (Note: the same color is also used to  
611 denote to same depth for both the model and observed data in Figures 2, 3, and 4 below.)  
612 The corresponding measured and modeled soil moisture is shown in Figure 2. These two  
613 figures indicate that the present model produces results that are similar to both the original  
614 *Campbell et al.* (1995) model and the observations. But they also indicate that the  $R_p =$   
615 4 mm simulation is superior to  $R_p = 1$  mm. Furthermore, comparing these two Figures  
616 with their counterparts in *Massman* [2012] clearly indicates that the non-equilibrium model  
617 is a substantial improvement over the (older) equilibrium model, a conclusion that is easily  
618 confirmed by comparing Figures 4 through 7 below with their equivalents in *Massman* [2012].

619 Figure 3 is a plot of the data trajectory (observed soil temperatures vs observed soil  
620 moistures for all the monitored depths). The model’s solution trajectories (for the same  
621 depths and the two  $R_p$  values) are shown in Figure 4. Comparing these two figures suggest  
622 that the model does a reasonable job of capturing the rapid vaporization of soil water at  
623 temperatures between 70 C and 90C (at least at the depths below about 10 mm). But the

624 present configuration of the model does not do as well at capturing the amplitude (amount)  
625 of the recondensing moisture ahead of the rapid drying nor the duration (or width of the  
626 amplitude) of the recondensation. Furthermore, when compared with observations (Figure  
627 3) the model does not fully capture the amount of unevaporated soil moisture that remains  
628 at temperatures  $\geq 150$  C. In this regard neither version of the model is significantly different  
629 from the other. But some of this “lack of precision” with the soil moisture simulation results  
630 in part by how the HCF was calibrated and will be examined in more detail in the next  
631 section.

632 Figure 5 compares the vertical profiles of the soil temperatures at the end of the laboratory  
633 experiment with those at the end of the two numerical simulations and Figure 6 makes a  
634 similar comparison for the volumetric soil moisture content. These figures also include the  
635 modeling results synchronized in time and space with the observations, which are included  
636 to make the model output more directly comparable to the observations. [Note: the final  
637 vertical profiles obtained from the laboratory experiment are not coincident in time with the  
638 measurements made at any other depth. This is a consequence of the experimental design,  
639 which required several minutes to complete one vertical scan for soil moisture.] Figure 5  
640 clearly indicates that the  $R_p = 4$  mm simulation does a better job of capturing the final  
641 temperature profile than does the  $R_p = 1$  mm simulation.

642 The difference between these two model simulations is less obvious with Figure 6.  
643 The final soil moisture profiles shown in this figure can be used to estimate the percentage  
644 of soil moisture evaporated and lost from the soil column at the end of the 90-minute ex-  
645 periment,  $E_{loss}$ . The laboratory observations suggests 31% was lost. The ( $R_p = 1$  mm; red)  
646 model simulation indicates a 31.4% loss and the corresponding (red) synchronized-model  
647 yielded a 33.8% loss. The ( $R_p = 4$  mm; blue) model simulation indicates a 34.6% loss and  
648 the corresponding (blue) synchronized-model yielded a 34.2% loss. Because the fully sam-

649 pled and synchronized model results give somewhat different percentage loss it is possible  
650 to conclude that the laboratory estimate of evaporative loss is likely imprecise because it is  
651 poorly resolved in time and space. So exact agreement between model and observations is,  
652 in general, unlikely. But it is possible to use the model itself to estimate the uncertainty in  
653 the observed moisture loss that is caused by this under-sampling. This is done by comparing  
654 and synthesizing all fully sampled model estimates of  $E_{loss}$  with all the corresponding syn-  
655 chronized model estimates. For the five experiments studied here this uncertainty, expressed  
656 as a fraction, is about  $\pm 0.03$ .

657 For the present Quincy Sand experiment this yields a fractional  $E_{loss} = 0.31 \pm 0.03$ , which  
658 in turn suggests that both the present simulations ( $R_p = 1$  mm and 4 mm) provide quite  
659 good estimates of the total water loss as well as the final profiles of soil moisture and may in  
660 essence really be indistinguishable. But combining these soil moisture results with the final  
661 temperature profiles suggest that the  $R_p = 4$  mm simulation is the preferred. In addition,  
662 the present model results are significantly better than the equilibrium model, which found  
663 that no water was lost during the experiment, a clearly implausible result! [Rather than  
664 actually transporting the evaporated water out of the soil column, the equilibrium model  
665 “pushed” the moisture deeper into the soil ahead of the evaporative front as discussed in the  
666 Introduction.] On the other hand, despite the fact that the present estimates of evaporative  
667 loss are clearly a major improvement over the equilibrium results, both the equilibrium and  
668 non-equilibrium model solutions produce a sharply delineated advancing drying front, which  
669 is reminiscent of a Stefan-like or moving-boundary condition problem (e.g., see *Whitaker*  
670 *and Chou* 1983-1984 or *Liu et al.* 2005). So neither simulation actually captures the final  
671 observed moisture profile behind the drying front.

672 Figure 7 shows the final (90-minute) modeled profiles of (a) the ( $R_p = 1$  mm) soil vapor  
673 density  $[\rho_v(z)]$ , equilibrium vapor density  $[\rho_{ve}(z)]$ , and the condensation term  $[\mathcal{K}_c(z)\rho_v(z)]$ ,



674 used with the non-equilibrium model source term,  $S_v$ : Equations (10) and (11)] and (b)  
 675 the ( $R_p = 4$  mm) soil vapor density [ $\rho_v(z)$ ]. The solid lines are model simulations with  $R_p$   
 676 = 1 mm; the dashed red line corresponds to the  $R_p = 4$  mm simulation. (For the sake of  
 677 simplicity only one curve is shown for  $R_p = 4$  mm simulation.) The maximum soil vapor  
 678 density occurs at about 40 mm where the evaporative source term is greatest, i.e., where  
 679  $\rho_{ve}(z) - \mathcal{K}_c(z)\rho_v(z)$  is maximal, and where the moisture gradient is steepest, which is just  
 680 ahead of the drying front (Figure 6). Furthermore, the  $\rho_v$  profile suggests that there are both  
 681 upward and downward diffusional fluxes of vapor away from the maximal evaporative source.  
 682 The upward-directed flux escapes through the soil surface and into the ambient environment  
 683 of the laboratory (the surface evaporative flux) and the downward-directed flux eventually  
 684 recondenses below of the dry front. The equilibrium model, on the other hand, produced  
 685 virtually no vapor gradient within the dry zone thereby contributing to the model's inability  
 686 to allow any moisture to escape (evaporate) from the modeling domain. Unfortunately, there  
 687 are no observations with which to check either models' predictions of vapor density. But,  
 688 although both models' results tend to agree that within the dry zone where temperatures  
 689 exceed the critical temperature for water (= 373.95 C) there should be a single phase fluid  
 690 that is significantly denser than water vapor near STP (e.g., *Pakala and Plumb* 2012), the  
 691 non-equilibrium model does predict a more realistic vapor gradient than the non-equilibrium  
 692 model.

693 If there is an implausibility with the present model it might be the soil vapor pressure,  
 694  $e_v$ , as shown in Figure 8. With either model simulation  $e_v$  at the top of the soil column  
 695 is between about 3 standard atmospheres ( $\approx 300$  kPa). This is a bit unexpected because  
 696 pressure at the open end of the column might be expected (at least by this author) to be close  
 697 to equilibrium with the ambient pressure ( $\approx 92$  kPa). Although there are no data against  
 698 which to check this result, there are other modeling results that lend some support to the

699 present predictions for  $e_v$ . First, (Figure 5 of) *Udell's* [1983] steady state model of a sand-  
700 water-steam system heated from above indicates that the environment within the modeling  
701 domain is likely to be super-saturated and that at a minimum  $e_v$  is greater than  $P_{atmos}$   
702 by  $\approx 5\%$ , but (depending on the algorithmic treatment of the saturation vapor pressure  
703 and the exact value of  $P_{atmos}$  he used for his simulations) it is also plausible to expect that  
704  $e_v \approx (2 - 5)P_{ST}$ . (Note that for *Udell's* [1983] simulations the maximum model temperature  
705 was about 180 C and that he also modeled advective velocity using Darcy's law.) Second,  
706 two different models of heated cement [*Dayan* 1982 and *Dal Pont et al.* 2011] indicate that  
707 near the top surface of the model domain  $e_v$  can display values of  $\approx (2 - 15)P_{ST}$ . The overall  
708 similarities between these three earlier models and the present non-equilibrium model make  
709 it impossible to completely invalidate the present model's predictions for  $e_v$ . Furthermore,  
710 the non-equilibrium model imposes no particular constraint on  $e_v$  – it is calculated using  
711 the ideal gas law and the profiles of vapor density and temperature, both of which appear  
712 plausible. Consequently, the somewhat surprising result shown in Figure 8 appears to be a  
713 natural consequence of the physics underlying the basic model equations: the conservation  
714 of mass and thermal energy.

#### 715 4.2.2 HCF – Quincy Sand

716 Figure 9 shows the hydraulic functions  $K_H^{cap}$ ,  $K_H^{film}$ ,  $|K_n^*|$ ,  $|K_n|$ , and  $|K_n^{surf}|$  as functions  
717 of soil moisture for the model simulation with  $R_p = 1$  mm. (Recall that the components  
718 of the hydraulic diffusivity are all negative, so this figure reflects only their absolute value,  
719 not their sign).  $K_H^{film}$  [assuming  $\mathcal{F}_w = 10^3$ , Equation (19)] was calculated after the model  
720 run using the model's solution for  $T_K$ ,  $\theta$ , and  $\psi$ . Because  $K_H^{film}$  did not actually contribute  
721 anything to any of the model runs for any of the five soil heating experiments (even for  $\mathcal{F}_w =$   
722  $10^4$ ), the present approach for evaluating it is sufficient. Consequently although  $|K_n|$  shown  
723 here is more properly termed  $|K_n^{cap}|$ , this distinction is rendered moot for the present study.

724 The values for  $m$  and  $n$  of  $K_R^{cap}$ , Equation (17), were  $m = 0.26$  and  $n = 1.80$  and were  
725 obtained by subjectively optimizing the model (with  $R_p = 1$  mm) to fit the data shown in  
726 Figures 1, 2, 5, and 6. In other words, it is possible to improve the model’s performance for  
727 either the temperature data or the soil moisture data individually, but not simultaneously.  
728 Any improvement in one set of observations ( $T_K$  or  $\theta$ ) comes at the expense of the model’s  
729 performance for the other variable. As a consequence of this optimization the model’s ability  
730 to fully capture the amplitude (amount) of soil moisture that evaporates and recondenses  
731 ahead of the drying front [Figures 3 and 4] has been sacrificed to improve the simulation of  
732 the soil temperatures. So the present numerical solution is a compromise between trying to  
733 fit two sets of data with a single “best” parameterization of *Assouline’s* [2009]  $K_R^{cap}$ . Similar  
734 compromises were required for other heating experiments as well. These particular optimal  
735 values for  $m$  and  $n$  were also found valid for the Boulder creek soil experiments; but for the  
736 Palousse B soil the optimal values were  $m = 0.29$  and  $n = 1.82$ .

737 Unfortunately, there are no independent confirmations for any values of  $m$  and  $n$  because  
738 no soil hydraulic conductivity data were (or ever have been) obtained for any of the soil  
739 samples used by *Campbell et al.* [1995]. Nor are any data likely at this point in time because  
740 the original samples were destroyed years ago (*G. S. Campbell*, personal communication,  
741 2015). At the time of these laboratory experiments the basic assumption that the original  
742 researchers made was that the heating and evaporation rates would be so fast as to preclude  
743 any (presumably much slower) liquid water transport associated with gradients in soil water  
744 potential. The present results appear to invalidate that assumption.

745 Although it is undeniably true that the present model is an improvement over the equi-  
746 librium model, the inclusion of the HCF within this non-equilibrium model (and its lack of  
747 inclusion in the equilibrium model) makes it difficult to conclude unambiguously that the  
748 improvement over equilibrium model is the sole consequence of the non-equilibrium assump-

749 tion. But the non-equilibrium model was tested in a mode that basically “turned off”  $K_R$   
750 and reduced  $K_n^{surf}$  by several orders of magnitude and still it yielded a solution (not shown)  
751 that simulated the soil temperatures and soil moisture observations better than did the equi-  
752 librium model. Furthermore, the non-equilibrium assumption will always remain superior to  
753 the equilibrium assumption for dry or extremely dry soils. Nonetheless, it remains unknown  
754 how much, if any, improvement in the equilibrium model’s performance is possible with the  
755 inclusion of a HCF.

756 Finally it should also be pointed out that, unlike  $K_R^{film}$ ,  $K_n^{surf}$  does contribute positively  
757 and significantly to the present model’s performance because without it the model can be-  
758 come unstable for very dry soils. Therefore,  $K_n^{surf}$  is a significant factor in the HCF’s overall  
759 contribution to the performance of the non-equilibrium model.

#### 760 4.2.3 Wet Palousse B

761 Figure 10 compares the measured (symbols) and modeled (lines) of soil temperatures  
762 during the Wet Palousse B heating experiment with the model run that includes the residual  
763 soil moisture,  $\theta_r$  (dashed), and that which does not (solid). Figure 11 compares the measured  
764 (symbols) and modeled (lines) of soil moisture during the same experiment. Figure 12 shows  
765 the two models’ solution trajectories, where the dashed line is the model run that includes  
766  $\theta_r$  and the solid line does not. These results suggest that the inclusion of the  $\theta_r$  in the model  
767 does not influence temperatures very much, but that the soil moisture dynamics are much  
768 better portrayed by the model with  $\theta_r$  than without it. In fact, the main difference between  
769 these two simulations is that the soil moisture that evaporates and recondenses ahead of the  
770 drying front is much less for the model that includes  $\theta_r$  than that which does not (Figure  
771 12). The significance of this aspect of the model’s performance is demonstrated in Figure 13,  
772 which, by comparing the observed Palousse B Wet trajectory data with the data from the  
773  $\theta_r$ -configured model, demonstrates that the  $\theta_r$ -configured model reproduces the observations

774 far more closely than does the model configured without  $\theta_r$ . The next two figures, Figures  
775 14 and 15, compare the final modeled and observed profiles of temperature and moisture  
776 for the Wet Palousse B experiment. These last two figures demonstrate (even more clearly  
777 than the previous figures) that including the dynamic soil moisture,  $\theta_r$ , has very little effect  
778 on the modeled soil temperatures, but that it does have a significant and positive effect on  
779 the modeled soil moistures. The predicted soil water loss from the  $\theta_r$ -configured model is  
780 almost exactly in agreement with the observed value of 28.8% and the modeled moisture  
781 profile below the drying front is also in almost perfect agreement with the observed data.  
782 The model without  $\theta_r$  allows much more evaporated moisture to diffuse downward and to  
783 recondense ahead of the drying front than does the  $\theta_r$  model; thereby underestimating the  
784 water loss by about half and significantly overestimating the amount of soil water in lower  
785 portion of the profile.

### 786 **4.3 Further Sensitivity Analyses**

787 The Quincy Sand and Palousse B results in general confirm that the non-equilibrium  
788 model's performance is enhanced (and quite significantly) with the incorporation of liquid  
789 water transport (HCF) and that its performance is sensitive to (and can be improved by)  
790 either or both (a) the infrared thermal conductivity,  $\lambda_s^{[2]}$ , through the volumetric pore radius,  
791  $R_p$ , and (b) the dynamical residual soil moisture,  $\theta_r(\psi, T_K)$ . Although these last two aspects  
792 of the present model may not apply equally to any given soil, there seems little doubt that  
793 they should be considered as potentially quite important for modeling soil moisture and  
794 temperature dynamics during heating of soil during fires.

795 The remainder of this section is a summary of various (secondary, but important) model  
796 sensitivity analyses performed with all soil heating experiments. The ultimate intent here is  
797 to shed light on which physical processes are relatively more important and to provide some  
798 guidance for further research.

### 799 4.3.1 The Source Term, Thermal Conductivity, and Surface Evaporation

800 There is little doubt that the present non-equilibrium model is an improvement over  
801 the equilibrium model of *Massman* (2012) and central to the success of the present model  
802 is the functional parameterization of the source term,  $S_v$ , and the related condensation  
803 coefficient,  $\mathcal{K}_c(T_K, \psi_n)$ . Basically  $\mathcal{K}_c$  was required to maintain model stability especially at  
804 high temperatures; without it the model was unstable and the dynamic between moisture  
805 and vapor was non-physical. Regarding  $\mathcal{K}_c$ , the model is weakly sensitive to the choice of the  
806 surface evaporation/condensation activation energy,  $E_{av}$ , providing it does not vary much  
807 outside the range of  $30 \text{ kJ mol}^{-1} \leq E_{av} \leq 40 \text{ kJ mol}^{-1}$ . On the other hand, from a systems  
808 perspective it is very difficult to infer much about the details of the (high-temperature)  
809 physical processes associated with  $\mathcal{K}_c$  or of the generality/universality of  $E_{av}$ , other than  
810 their apparent existence and utility to the present model. The most effective value for the  
811 scaling parameter,  $S_*^{[M]}$ , was within the range of about 0.5 to 1. The Novak model of the  
812 source term,  $S_v^{[N]}$ , also required the same  $\mathcal{K}_c$ , but the additional temperature dependency of  
813  $S_v^{[N]}$  over  $S_v^{[M]}$  forced the soil moisture to evaporate at slightly lower temperatures (therefore  
814 sooner) than shown in Figure 4 for the Quincy Sand  $S_v^{[M]}$ -configured model.  $S_v^{[N]}$  also  
815 eliminated an initial transient/instability (not shown) that occurred with the Quincy Sand  
816  $S_v^{[M]}$  solution. Otherwise, the differences between  $S_v^{[N]}$  and  $S_v^{[M]}$  were not significant.

817 It should not be surprising that the model is sensitive to soil thermal conductivity,  $\lambda_s$ ; but  
818 it was somewhat surprising that the model is as sensitive to  $\lambda_s^{[2]} [R_p]$  as it is. Both *Durany*  
819 *et al.* [2010] and *Massman* [2102] found that  $\lambda_s^{[2]}$  only contributed for relatively porous soils,  
820 i.e.,  $R_p > 10^{-3}$  m. In the present study the model temperatures could often be “fine tuned”  
821 (improved) even for relatively small values of  $R_p$ . Therefore, in general, it seems unwise to  
822 ignore  $\lambda_s^{[2]}$ , at least when modeling soil heating during fires.

823 The most important parameter controlling surface evaporation rate is the surface transfer

824 coefficient  $C_E$ , to which the model is reasonably sensitive. In particular (and similar to  
825 *Massman's* 2012 results), the best (maximal) values of  $C_E$  were universally about  $10^{-3}$  m  
826  $s^{-1}$  and values much above this caused the model to become unstable. Values well below  
827 these values (and closer to the theoretical value of  $10^{-4}$  m  $s^{-1}$ ) did not produce results much  
828 different than those resulting from  $C_E = 10^{-3}$  m  $s^{-1}$ . Nevertheless,  $C_E$  does play a weak role  
829 in determining the soil surface temperature,  $T_{K0}$ , and therefore can influence the magnitude  
830 of the surface convective heat flux – Equation (24) – and  $\lambda_{s0}^{[2]}(T_{K0})$ , which can influence the  
831 soil temperatures to some depth below the soil surface.

### 832 **4.3.2 Water Retention Curves and Hydraulic Conductivity Functions**

833 The two other WRCs tested for model performance were *Groenevelt and Grant* [2004]  
834 (GG04) and *Fredlund and Xing* [1994] (FX94). But prior to implementing them in the model  
835 they were both calibrated to be numerically similar near the dry end ( $\theta \leq 0.03$ ) of Equation  
836 (15). Their performance was initially tested with the *Assouline* [2009] HCF, Equation (17).  
837 In addition, and as listed in section 2.2.5, besides Equation (17) four other HCFs were also  
838 tested. Although not all pairings of WRCs and HCFs were tested against every heating ex-  
839 periment, the following conclusions seem relatively robust: (1) once calibrated to the present  
840 data set, the *Brooks and Corey* [1964] HCF performed at least as well as Equation (17), but  
841 with only one parameter rather than two, while the other three HCFs gave somewhat less  
842 satisfying results and sometimes would even produce an instability; (2) the FX94 WRC often  
843 produced an instability, but its performance was also somewhat dependent upon which HCF  
844 was used with it; and (3) the GG04 WRC and associated HCFs did perform better the FX94,  
845 but overall, it did not perform as well as the present model configuration with Equation (15)  
846 for the WRC and Equation (17) for the HCF. In general the only guidance offered here is  
847 that some care must be given to choice of WRCs and HCFs because the modeling results  
848 can be quite dependent upon the choices made.

849 Universal to all of HCFs tested here is  $K_n^{surf}$  [i.e.,  $V_{\theta,surf}$  and its scaling parameter  $D_{\theta s0}$ :  
 850 see Equations (20) and (21)], which as explained above was incorporated into the hydraulic  
 851 diffusivity,  $K_n^*$  [see Equation (6) and the related discussion]. The model’s performance was  
 852 relatively insensitive to the exact value of  $D_{\theta s0}$  and  $D_{\theta s0} \approx 10^{-10} \text{ m}^2\text{s}^{-1}$  is as good a default  
 853 value as any other value. Furthermore, the inclusion of  $V_{\theta,surf}$  (soil moisture movement  
 854 associated with water molecules “hopping or skipping” along the soil and water surfaces)  
 855 did provide model stability when the soil moisture reached extremely low values. Including  
 856 film flow,  $K_r^{film}$  – Equations (18) and (19), brought no discernible benefit to the model’s  
 857 performance. But that does not mean that under more benign conditions that it would  
 858 not. Consequently it seems reasonable to further investigate the possibility of film flow when  
 859 modeling less extreme conditions.

### 860 4.3.3 Different Soils with Different Initial Conditions

861 Of the remaining three heating experiments only Wet Boulder creek, which had an initial  
 862 soil saturation level of about 50%, showed anything unexpected. In general, the model was  
 863 able to capture the observed soil temperatures and temperature dynamics extremely well,  
 864 even better than shown in either Figure 5 (Quincy Sand) or Figure 14 (Palousse B). But,  
 865 regardless of any adjustments to any of the model parameters the model consistently under-  
 866 estimated the total amount of water evaporated (by about half), thereby also overestimating  
 867 the amount of recondensing water ahead of the drying front (see the Wet Palousse B model  
 868 run without  $\theta_r$ , Figure 15, as an example). On the other hand, the model was able to capture  
 869 the complete drying ( $\theta \equiv 0$ ) of the top 30 mm of the soil column during the Wet Boulder creek  
 870 experiment, whereas the Quincy Sand (Figure 6) and Palousse B (Figure 15) experiments  
 871 indicated some residual soil moisture ( $0 < \theta < 0.025$ ) within the model’s predicted dry zone.  
 872 The model’s performance was noticeably degraded when  $\theta_r$  was included and it was also  
 873 quite sensitive to the choice of  $R_p$ , so much so that best model fit to temperatures required



874 that  $R_p = 0$ , i.e., that  $\lambda_s^{[2]}$  be excluded from the model. Nonetheless, the cause for this  
875 unexpected divergence between the modeling and observed soil moisture during this heating  
876 experiment is not understood. For the present it can only be surmised that the model's  
877 description of evaporative dynamics of soil moisture, and possibly the transport of water  
878 (both liquid and vapor), is still incomplete.

#### 879 **4.3.4 The advective velocity, $u_{vl}$**

880 Unlike with the companion model [Massman 2012], the present model did not require  
881 reducing the magnitude of  $u_{vl}$  in order to maintain model stability, which again reinforces  
882 the impression that the present non-equilibrium model is an improvement over equilibrium  
883 model. Nonetheless, the present model can produce extraordinary gradients of vapor density  
884 and vapor pressure, which begs the question of whether such gradients could induce other  
885 types of mass transport than that captured by the present formulation of  $u_{vl}$ , Equation  
886 (9). This was tested by using a model for Darcy's Law type formulation based on the  
887 assumption that the advective velocity is proportional to the vapor pressure gradient ( $u_{vl} \propto$   
888  $-\partial e_v / \partial z$ ). This formulation was tested by incorporating it into the model (excluding  $\theta_r$ ).  
889 But the model became unstable because mathematically it was strongly hyperbolic, rather  
890 than predominantly parabolic. Further modeling development and parameterization of  $u_{vl}$   
891 and vapor transport in general are well beyond the intent of the present study. But it is  
892 still possible to conclude that such exploration is warranted and could help improve model  
893 performance. Finally, it should be noted that the model's performance was degraded when  
894  $u_{vl}$  was excluded from the model.

### 895 **5. Summary and Recommendations**

896 This study has developed and tested a non-equilibrium (liquid to vapor phase change)  
897 model for simulating heat and moisture flow in soils during fires; but the model does assume  
898 thermal equilibrium. By and large the simulations of soil temperature and moisture are

899 not only credible, but often quite good. In general, all model results showed a significant  
900 improvement over all comparable results from the companion equilibrium model of *Massman*  
901 [2012].

902 The principal reason for the present model’s success is the incorporation of a dynamic  
903 condensation coefficient,  $\mathcal{K}_c$  (parameterized as a function of temperature and soil water po-  
904 tential), into the non-equilibrium evaporative source term,  $S_v$ ; both of which are modeled  
905 after the Hertz-Knudsen Equation. Physically  $\mathcal{K}_c$  suppressed condensation in favor of evapo-  
906 ration at high temperatures and soil water potentials, which in turn insured model stability.  
907 Furthermore, the non-equilibrium assumption also seemed to have improved the parameter-  
908 ization (and performance) of the mass transport associated with the advective velocity,  $u_{vl}$ ,  
909 relative to the model’s of *Massman* [2012] and *Campbell et al.* [1995]. The model’s perfor-  
910 mance was further and significantly enhanced by the inclusion of a hydraulic conductivity  
911 function (HCF) for liquid water transport, which was calibrated here by “fitting” the HCF  
912 parameters to ensure that the model optimally reproduced the observed temperature and  
913 moisture dynamics. This fitting procedure was necessary because no data are (nor will be)  
914 available for the soil samples used in the laboratory heating experiments [*Campbell et al.*  
915 1995]. Another important (and novel) feature of the model is the inclusion of a dynamic  
916 residual soil moisture  $\theta_r$ , also parameterized as a function of temperature and soil water po-  
917 tential, which is introduced into the model in an attempt to capture the long evaporative tail  
918 that seems to require temperatures well beyond 100 C in order to evaporate at all. Physically  
919  $\theta_r$  is intended to represent the strongly bound soil moisture, which for the present purposes  
920 is conceptualized as a mono-layer. Including  $\theta_r$  was sometimes, but not always, beneficial  
921 to model performance. So it seems worthy of further consideration and possible refinement  
922 in any future studies of a similar nature. Finally, the model is also sensitive to the thermal  
923 infrared radiation component to the soil’s thermal conductivity [ $\lambda_s^{[2]}$ : Equation (14)], which

924 increases the thermal conductivity within the pore space of the soil as temperature increases.  
925 It is recommended that this term also be included and further tested when evaluating any  
926 future models describing the heating soils to high temperatures.

927 In general, the model simulates the observed soil temperatures quite well. It is often  
928 slightly less precise for soil moisture and the best simulations were usually a compromise  
929 between faithfully representing the observed soil temperatures or the observed soil moistures.  
930 Nonetheless, the model does capture reasonably well many observed features of the soil  
931 moisture dynamics, viz., it simulates an increase in soil moisture ahead of the drying front  
932 (due to the condensation of evaporated soil water at the front) and the hiatus in the soil  
933 temperature rise during the strongly evaporative stage of the soil drying. Furthermore, the  
934 model also captures the observed rapid evaporation of soil moisture that occurs at relatively  
935 low temperatures (50-90 C), as well as some aspects of the long evaporative tail associated  
936 with strongly bound soil moisture. But, the model also displays a tendency to predict a  
937 greater depth of the drying front than suggested by the observations.

938 Sensitivity analyses (SAs) were also performed with different formulations for the water  
939 retention curve, soil hydraulic conductivity function, one variant of the present evaporative  
940 source term,  $S_v$ , and different soil types with different initial conditions. The principal  
941 conclusion from these SAs is that some care (and testing) must be given to the selection of  
942 the WRC and HCF, as not all of them performed equally well. Some further investigations  
943 into the modeling benefit of film flow as part of the HCF also seems warranted. The two  
944 forms of  $S_v$  tested here performed about the same. And the model's performance (at least for  
945 soil moisture) was poorest compared to the experiment with the highest initial soil moisture  
946 content. No obvious explanation for this 'under-performance' could be found, so it seems  
947 worthwhile to further test the model for high initial saturation conditions. Finally, it is  
948 important to test the present model's performance and its associated parameterizations

949 (particularly the WRC and HCF) against laboratory data and field data associated with  
950 daily cycles of soil heating and moisture transport.

951 **Acknowledgments**

952 All modeling code and data used in this paper are freely available from the author.  
953 I would like to thank Gaylon S. Campbell for providing the laboratory data used in this  
954 study, as well as James W. Thomas for his insights into and discussions of the mathematical  
955 and numerical issues I encountered during the development of this model and Marcia L.  
956 Huber and Allan H. Harvey for various discussions concerning the thermophysical properties  
957 of water and aid with the published resources used in parameterizing the self diffusion of  
958 water vapor.

## References

- [1] Assouline, S.: A model for the relative hydraulic conductivity based on the water retention curve, *Water Resour. Res.*, 37, 265-271, 2001.
- [2] Assouline, S. and Or, D.: Conceptual and parametric representation of hydraulic properties: A review, *Vadose Zone Journal*, 12, 1-20, doi:10.2136/vzj2013.07.0121, 2013.
- [3] Aston, A. R. and Gill, A. M.: Coupled soil moisture, heat and water vapour transfers under simulated fire conditions, *Australian J. Soil Res.*, 14, 55-66, 1976.
- [4] Bauer, T. H.: A general analytical approach toward the thermal conductivity of porous media, *Int. J. Heat Mass Transfer*, 36, 4181-4191, 1993.
- [5] Bear, J.: *Dynamics of Fluids in Porous Media*, American Elsevier Pub. Co, New York, NY, USA, 1972.
- [6] Bridge, L., Bradean, R., Ward, M. J., and Wetton, B. R.: The analysis of a two-phase zone with condensation in a porous medium, *J. Eng. Math.*, 45, 247-268, 2003.
- [7] Brooks, R. H. and Corey, A. T.: *Hydraulic properties of porous media*, Hydrology Paper 3, Colorado State University, Fort Collins, CO, USA, 1964.
- [8] Bücker, D., Span, R., and Wagner W.: Thermodynamic property models for moist air and combustion gases, *J. Eng. Gas Turbines Power*, 125, 374-384, 2003.
- [9] Campbell, G. S.: *Soil Physics with BASIC*, Elsevier, New York, NY, USA, 1985.
- [10] Campbell, G. S., Jungbauer Jr., J. D., Bidlake, W. R., and Hungerford, R. D.: Predicting the effect of temperature on soil thermal conductivity, *Soil Science*, 158, 307-313, 1994.

- 980 [11] Campbell, G. S., Jungbauer Jr., J. D., Bristow, K. L., and Hungerford, R. D.: Soil  
981 temperature and water content beneath a surface fire, *Soil Science*, 159, 363-374, 1995.
- 982 [12] Campbell, G. S., and Shiozawa, S.: Prediction of hydraulic properties of soils using  
983 particle-size distribution and bulk density data, in *Indirect methods for estimating the*  
984 *hydraulic properties of unsaturated soils*, edited by M. Th. van Genuchten, University  
985 of California, Riverside, CA, 317-328, 1992.
- 986 [13] Costa, V. A. F., Mendoça M. L., and Figueiredo, A. R.: Modeling and simulation of  
987 wetted porous thermal barriers operating under high temperature or high heat flux,  
988 *Int. J. Heat Mass Trans.*, 51, 3342-3354, 2008.
- 989 [14] Constanza-Robinson, M. S., and Brusseau, M. L.: Air-water interfacial areas in un-  
990 saturated soils: evaluation of interfacial domains, *Water Resour. Res.*, 38 (10), 1195,  
991 doi:10.1029/2001WR000738, 2002.
- 992 [15] Dal Pont, S., Meftah, F., and Schrefler, B. A.: Modeling concrete under severe condi-  
993 tions as a multiphase material, *Nuclear Engineering and Design*, 241, 562-572, 2011.
- 994 [16] Danielewicz-Ferchmin, I., and Mickiewicz, A. R.: Water Density in the Double Layer,  
995 *J. Phys. Chem.*, 100, 17281-17286, 1996.
- 996 [17] Dayan, A.: Self-similar temperature, pressure and moisture distribution within an  
997 intensely heated porous half space, *J. Heat Trans.*, 25, 1469-1476, 1982.
- 998 [18] de Vries, D. A.: Simultaneous transfer of heat and moisture in porous media, *EOS*  
999 *Trans. AGU*, 39, 909-916, 1958.
- 1000 [19] de Vries, D. A.: Thermal properties in soils, in *Physics of Plant Environment*, edited  
1001 by W. R. van Wijk, North Holland Publishing Co., Amsterdam, 201-255, 1963.

- 1002 [20] di Blasi, C.: Simultaneous heat, mass, and momentum transfer during biomass drying,  
1003 in *Developments in Thermochemical Biomass Conversion*, edited by A. V. Bridgwater  
1004 and D.G.B. Boocock, Springer Science+Business Media, Dordrecht, 117-131, 1997.
- 1005 [21] Durany, J., Fraga, B., and Vargas, F.: Physical modelling and numerical simulation  
1006 of soil heating under forest fire conditions, in *Forest Fire Research*, edited by D. X.  
1007 Viegas, ADAI/CEIF, Coimbra, Portugal, paper no. 263 of the attached CD, 2010.
- 1008 [22] Fernández, D. P., Goodwin, A. R. H., Lemmon, E. W., Levelt Sengers, J. M. H. and  
1009 Williams, R. C.: A Formulation for the static permittivity of water and steam at  
1010 temperatures from 238 K to 873 K at pressures up to 1200 MPa, including derivatives  
1011 and Debye-Hückel coefficients, *J. Phys. Chem. Ref. Data*, 26, 1125-1166, 1997.
- 1012 [23] Fredlund, D. G. and Xing, A: Equations for the soil-water characteristic curve, *Can.*  
1013 *Geotech. J.*, 31, 521-532, 1994.
- 1014 [24] Gawin, D., Majorana, C. E., and Schrefler, B. A.: Numerical analysis of hydro-thermal  
1015 behavior and damage of concrete at high temperatures, *Mech. Cohes.-Frict. Materials*,  
1016 4, 37-74, 1999.
- 1017 [25] Grant, C. D., Groenevelt, P. H., and Robinson, N. I.: Application of the Grant-  
1018 Groenevelt soil water retention model to predict the hydraulic conductivity, *Australian*  
1019 *J. Soil Res.*, 48, 447-458, 2010.
- 1020 [26] Groenevelt, P. H. and Grant, C. D.: A new model for the soil-water retention curve  
1021 that solves the problem of residual water contents, *European J. Soil Sci.*, 55, 479-485,  
1022 2004.
- 1023 [27] Gupta, H. V. and Nearing, G. S.: Debates—The future of hydrological sciences: A  
1024 (common) path forward? Using models and data to learn: A systems theoretic per-

- 1025        spective on the future of hydrological science, *Water Resour. Res.*, 50, 5351-5359,  
1026        doi:10.1002/2013WR015096, 2014.
- 1027 [28] Harvey, A. H. and Friend, D. G.: Physical properties of water, in *Aqueous systems*  
1028        at elevated temperatures and pressures: physical chemistry of water, steam and hy-  
1029        drothermal solutions, edited by D. A. Palmer, R. Fernández-Prini and A. H. Harvey,  
1030        Elsevier, Amsterdam, The Netherlands, 1-27, 2004.
- 1031 [29] Hellmann, R., Bich, E., Vogel, E., Dickinson, A. S., and Vesovic, V.: Calculation of  
1032        the transport and relaxation properties of dilute water vapor, *J. Chem. Phys.*, 131,  
1033        014303; doi: 10.1063/1.3158830, 2009.
- 1034 [30] Huber, M. L., Perkins, R. A., Laeseche, A., Friend, D. G., Sengers, J. V., Assael, M. J.,  
1035        Metaxa, I. N., Vogel, E., Mareš, R., and Miyagawa, K.: New international formulation  
1036        for the viscosity of H<sub>2</sub>O, *J. Phys. Chem. Ref. Data*, 38, 101-125, 2009.
- 1037 [31] Huber, M. L., Perkins, R. A., Friend, D. G., Sengers, J. V., Assael, M. J., Metaxa, I.  
1038        N., Miyagawa, K., Hellmann, R., and Vogel E.: New international formulation for the  
1039        thermal conductivity of H<sub>2</sub>O, *J. Phys. Chem. Ref. Data*, 41, 033102,  
1040        <http://dx.doi.org/10.1063/1.4738955>, 2012.
- 1041 [32] IAPWS [The International Association for the Properties of Water and Steam]: Re-  
1042        vised release on the IAPWS industrial formulation 1997 for the thermodynamic prop-  
1043        erties of water and steam, available at <http://www.iapws.org>, (last access: May 24,  
1044        2013), 2007.
- 1045 [33] Jacobs, A. F., and Verhoef, A.: Soil evaporation from sparse natural vegetation esti-  
1046        mated from Sherwood numbers, *J. Hydrol.*, 188-189, 443-452, 1997.



- 1047 [34] Jovanović, J. D., Kneženić-Stevanović, A. B., and Grozdanić, D. K.: An empirical  
1048 equation for temperature and pressure dependence of liquid heat capacity, *J. Taiwan*  
1049 *Inst. Chem. Eng.*, 40, 105-109, 2009.
- 1050 [35] Kadoya, K., Matsunaga, N., and Nagashima, A.: Viscosity and thermal conductivity  
1051 of dry air in the gaseous phase, *J. Phys. Chem. Ref. Data*, 14, 947-970, 1985.
- 1052 [36] Kapoor, A., Yang, R. T., and Wong, C.: Surface diffusion, *Catalysis Reviews – Science*  
1053 *and Engineering*, 31, 129-214, 1989.
- 1054 [37] Ki, H., Mohanty, P. S., and Mazumder, J.: A numerical method for multiphase in-  
1055 compressible thermal flows with solid-liquid and liquid-vapor phase transformations,  
1056 *Numerical Heat Transfer, Part B: Fundamentals*, 48, 125-145, 2005.
- 1057 [38] Kon, M., Kobayashi, K. and Watanabe, M.: Method of determining kinetic bound-  
1058 ary conditions in net evaporation/condensation, *Physics of Fluids (1994-present)*, 26,  
1059 072003, doi: 10.1063/1.4890523, 2014.
- 1060 [39] Kozłowski, T.: Modulated Differential Scanning Calorimetry (MDSC) studies on low-  
1061 temperature freezing of water adsorbed on clays, apparent specific heat of soil water  
1062 and specific heat of dry soil, *Cold Regions Sci. Tech.*, 78, 89-96, 2012.
- 1063 [40] Lynch, D. R.: Numerical partial differential equations for environmental scientists and  
1064 engineers, Springer, New York, NY, 2005.
- 1065 [41] Marrero, T. R. and Mason, E. A.: Gaseous diffusion coefficients, *J. Phys. Chem. Ref.*  
1066 *Data*, 1, 3-118, 1972.

- 1067 [42] Massman, W. J.: Modeling soil heating and moisture transport under extreme condi-  
1068 tions: Forest fires and slash pile burns, *Water Resour. Res.*, 48, W10548,  
1069 doi:10.1029/2011WR011710, 2012.
- 1070 [43] Medveď, I. and Černý, R.: Surface diffusion in porous media: A critical review, *Mi-  
1071 croporous and Mesoporous Materials*, 142, 405-422, 2011.
- 1072 [44] Miles, R. E. H., Reid, J. P., and Rüpinen, I.: Comparison of approaches for measuring  
1073 the mass accommodation coefficient for the condensation of water and sensitivities to  
1074 uncertainties in thermophysical properties, *J. Phys. Chem. A*, 116, 10810-10825, 2012.
- 1075 [45] Milly, P. C. D.: Moisture and heat-transport in hysteretic, inhomogeneous porous  
1076 media: A matric head-based formulation and a numerical model, *Water Resour. Res.*,  
1077 18, 489-498, 1982.
- 1078 [46] Moldrup, P. T., Olesen, D. E., Roslton, D. E., and Yamaguchi, T.: Modeling diffusion  
1079 and reactions in soils: VII. Predicting gas and ion diffusivity in undisturbed and sieved  
1080 soils, *Soil Sci.*, 162, 632-640, 1997.
- 1081 [47] Novak, M. D.: Dynamics of the near-surface evaporation zone and corresponding effects  
1082 on the surface energy balance of a drying soil, *Ag. For. Meteorol.*, 150, 1358-1365, 2010.
- 1083 [48] Novak, M. D.: Comment on “Evaporation from soils under thermal boundary  
1084 conditions: Experimental and modeling investigation to compare equilibrium- and  
1085 nonequilibrium-based approaches” by Kathleen M. Smits, Abdullah Cihan, Toshi-  
1086 hiro Sakaki, and Tissa H. Illangasekare, *Water Resources Research*, 48, W05549,  
1087 doi:10.1029/2011WR011393, 2012.

- 1088 [49] Ouedraogo, F., Cherblanc, F., Naon, B., and Bénet, J.-C.: Water transfer in soil at  
1089 low water content. Is the local equilibrium assumption still appropriate?, *J. Hydrology*  
1090 492, 117-127, 2013.
- 1091 [50] Pakala, V. K. C. and Plumb, O. A.: High intensity drying in porous materials, *J.*  
1092 *Thermal Sci. Eng. Appls.*, 4, 021010, doi:/10.1115/1.4006275, 2012.
- 1093 [51] Philip, J. R. and de Vries, D. A.: Moisture movement in porous materials under  
1094 temperature gradients, *EOS Trans. AGU*, 38, 222-232, 1957.
- 1095 [52] Sato, H.: An equation of state for the thermodynamic properties of water in the liquid  
1096 phase including the metastable state, in *Properties of Water and Steam Proceedings*  
1097 *of the 11<sup>th</sup> International Conference*, edited by M. Píchal and O. Šifner, Hemisphere  
1098 Publishing Company, New York, NY, USA, 48-55, 1990.
- 1099 [53] Shiozawa, S., and Campbell, G. S.: On the calculation of mean particle diameter and  
1100 standard deviation from sand, silt, and clay fractions, *Soil Science*, 152, 427-431, 1991.
- 1101 [54] Skopp, J.: Oxygen uptake and transport in soils: analysis of the air-water interfacial  
1102 area, *Soil Sci. Soc. Amer. J.*, 49, 1327-1331, 1985.
- 1103 [55] Smits, K. M., Cihan, A., Soshihiro, T., and Illangasekare, T. H.: Evaporation from  
1104 soils under thermal boundary conditions: Experimental and modeling investigation to  
1105 compare equilibrium- and nonequilibrium-based approaches, *Water Resour. Res.*, 47,  
1106 W05540, doi:10.1029/2010WR009533, 2011.
- 1107 [56] Smits, K. M., Cihan, A., Ngo, V. V., and Illangasekare T. H.: Reply to comment  
1108 by Michael D. Novak on “Evaporation from soils under thermal boundary conditions:

- 1109 Experimental and modeling investigation to compare equilibrium- and nonequilibrium-  
1110 based approaches”, *Water Resour. Res.*, 48, W05550, doi:10.1029/2011WR011609,  
1111 2012.
- 1112 [57] Somayajulu, G. R.: New equations for enthalpy of vaporization from the triple point  
1113 to the critical point, *Int. J. Thermophysics*, 9, 567-575, 1988.
- 1114 [58] Thomas, J. C.: *Numerical partial differential equations: finite difference methods*,  
1115 Springer, New York, NY, USA, 1985.
- 1116 [59] Tsilingiris, P. T.: Thermophysical transport properties of humid air at temperature  
1117 range between 0 and 100 C, *Energy Conservation and Management*, 49, 1098-1110,  
1118 2008.
- 1119 [60] Tsuruta, T. and Nagayama, G.: Molecular dynamics studies on the condensation  
1120 coefficient of water, *J. Phys. Chem. B*, 108, 1736-1743, 2004.
- 1121 [61] Udell, K. S.: Heat transfer in porous media heated from above with evaporation,  
1122 condensation, and capillary effects, *J. Heat Trans.*, 105, 485-492, 1983.
- 1123 [62] Van Genuchten, M. Th. and Nielsen, D. R.: On describing and predicting the hydraulic  
1124 properties of unsaturated soils, *Annales Geophysicae*, 3, 615-628, 1985.
- 1125 [63] Vargaftik, N. B., Volkov, B. N. and Voljak, L. D.: International tables of the surface  
1126 tension of water, *J. Phys. Chem. Ref. Data*, 12, 817-820, 1983.
- 1127 [64] Wagner, W. and Pruess, A.: The IAPWS formulation 1995 for the thermodynamic  
1128 properties of ordinary water substance for general and scientific use, *J. Phys. Chem.*  
1129 *Ref. Data*, 31, 387-535, 2002.

- 1130 [65] Whitaker, S.: Simultaneous heat, mass and momentum transfer in porous media: a  
1131 theory of drying, *Adv. Heat Trans.*, 13, 119-203, 1977.
- 1132 [66] Whitaker, S. and Chou, W. T.-H.: Drying granular porous media – Theory and ex-  
1133 periment, *Drying Technol.*, 1, 3-33, 1983-1984.
- 1134 [67] Yaws, C.: *Handbook of Transport Property Data*, Gulf Publishing Company, Houston,  
1135 TX, USA, 1985.
- 1136 [68] Yoshida, K., Matubayasi, N., and Nakahara, M.: Self-diffusion of supercritical water  
1137 in extremely low-density region, *J. Chem. Phys.*, 125, 074307; doi: 10.1063/1.2333511,  
1138 2006.
- 1139 [69] Yoshida, K., Matubayasi, N., and Nakahara, M.: Erratum: Self-diffusion of super-  
1140 critical water in extremely low-density region [*J. Chem. Phys.* 125, 074307 (2006)], *J.*  
1141 *Chem. Phys.*, 126, 089901; doi: 10.1063/1.2372501, 2007.
- 1142 [70] Zhang, Z. F.: Soil water retention and relative permeability for conditions from oven-  
1143 dry to full saturation, *Vadose Zone J.*, 10, 1299-1308, doi: 10.2136/vzj2011.0019, 2011.

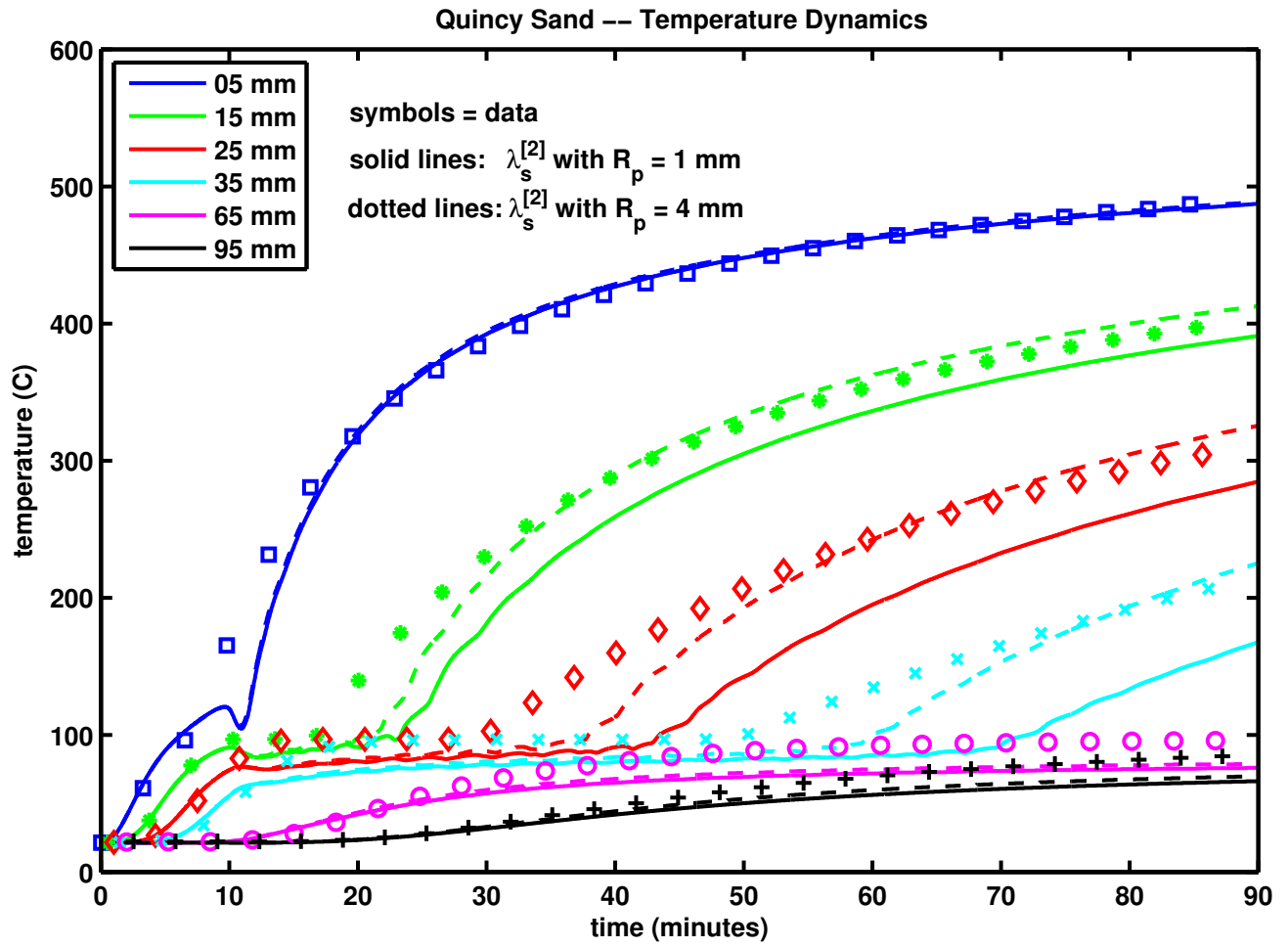


Figure 1:

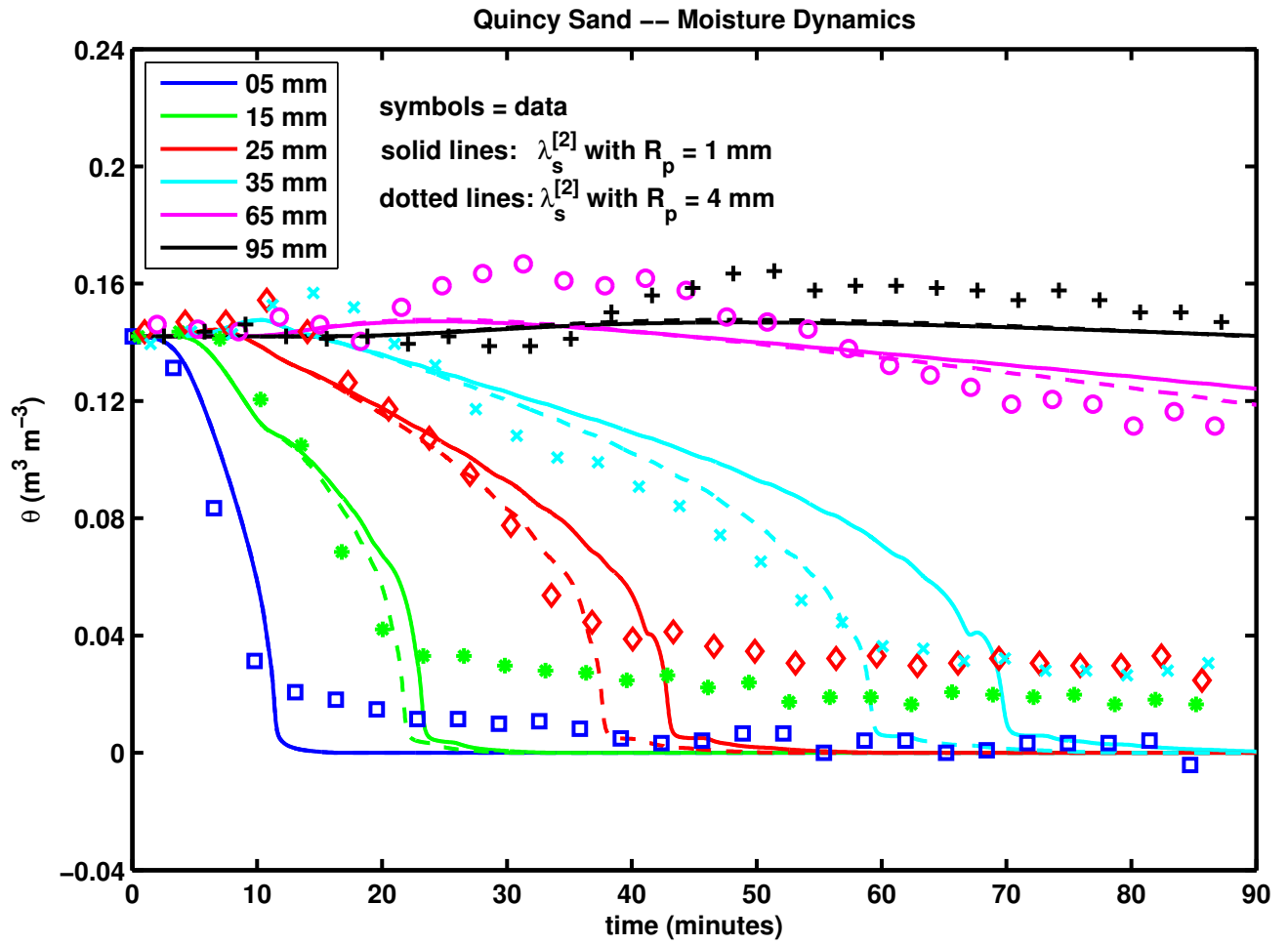


Figure 2:

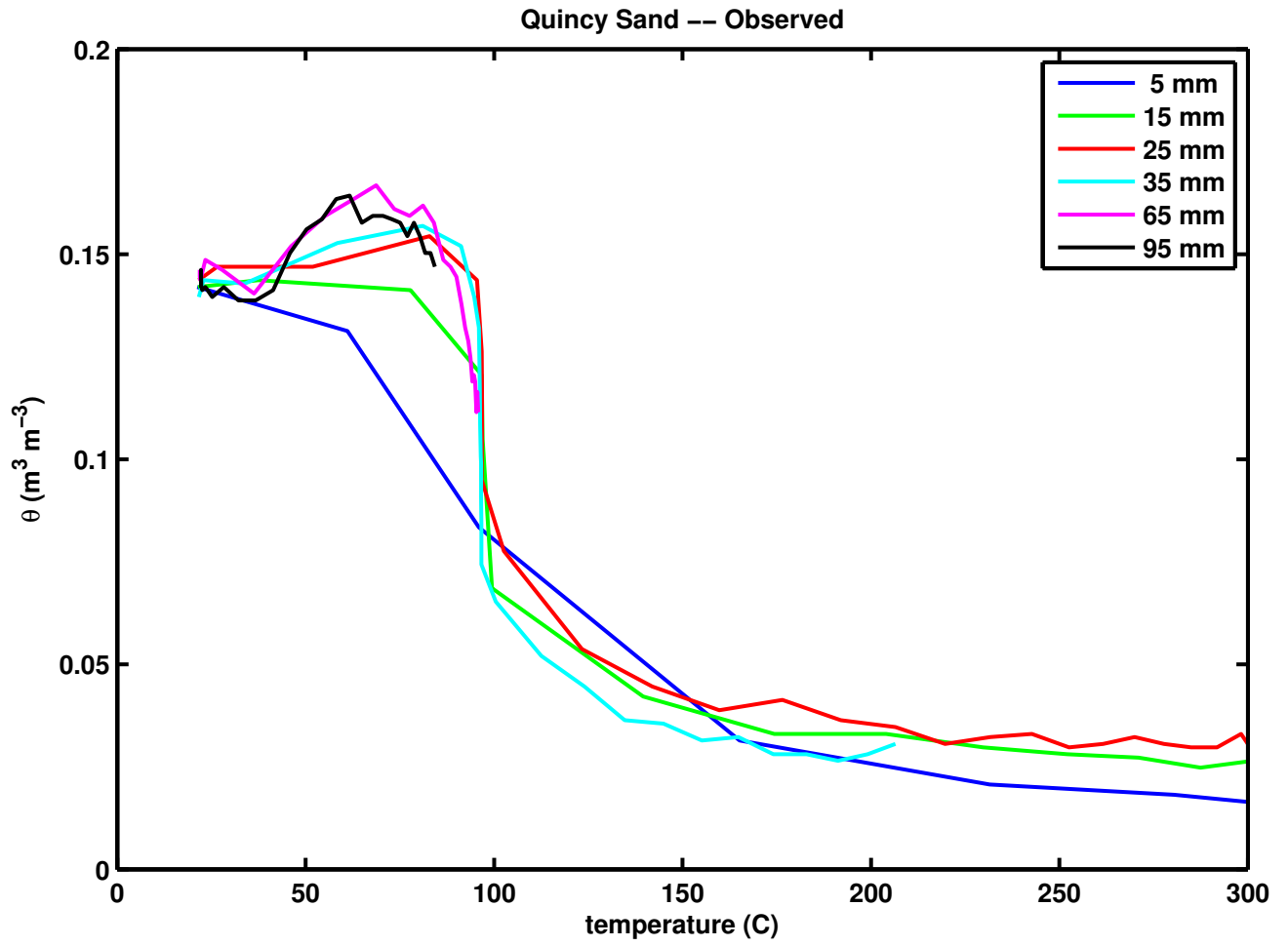


Figure 3:



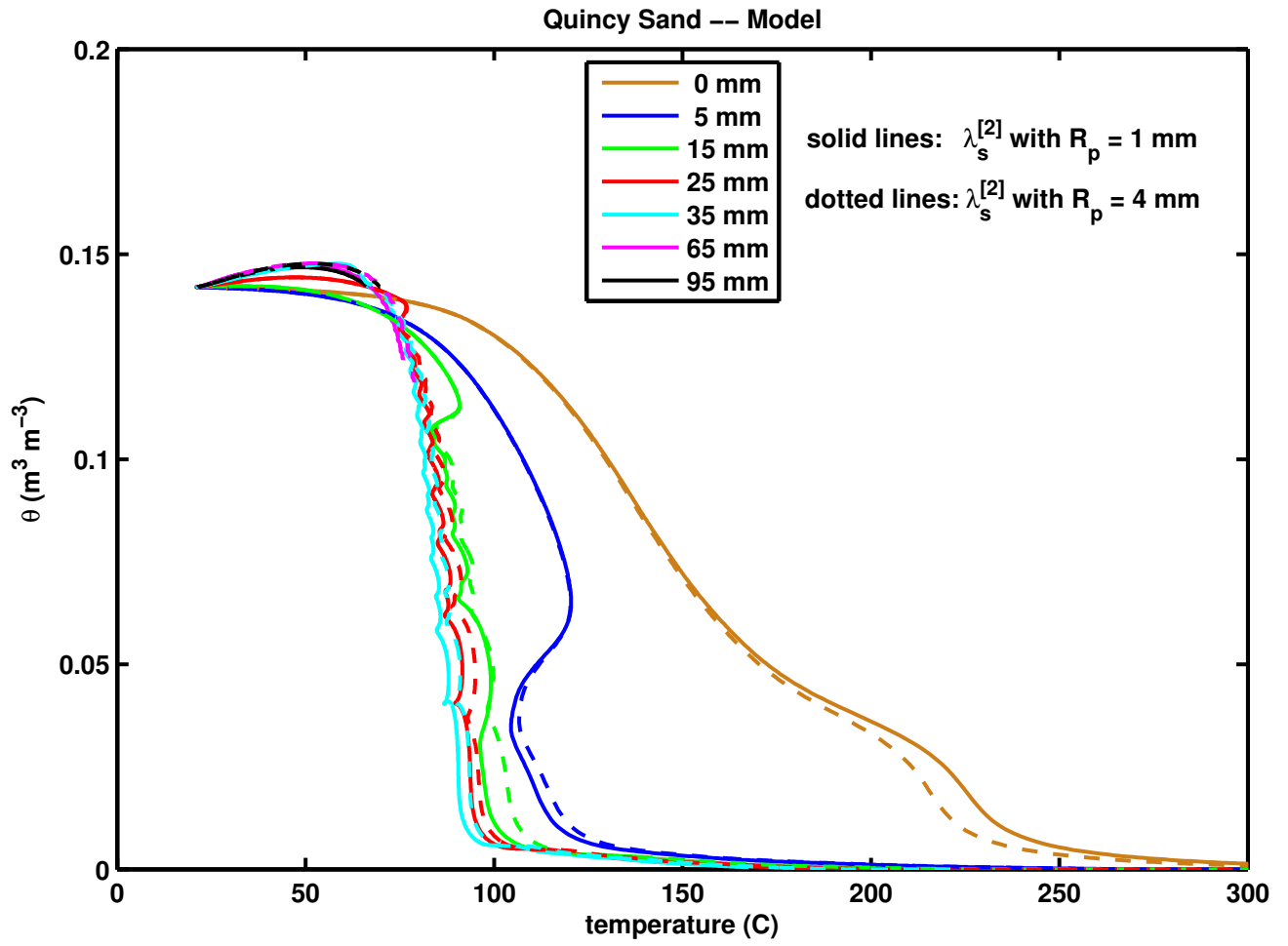


Figure 4:

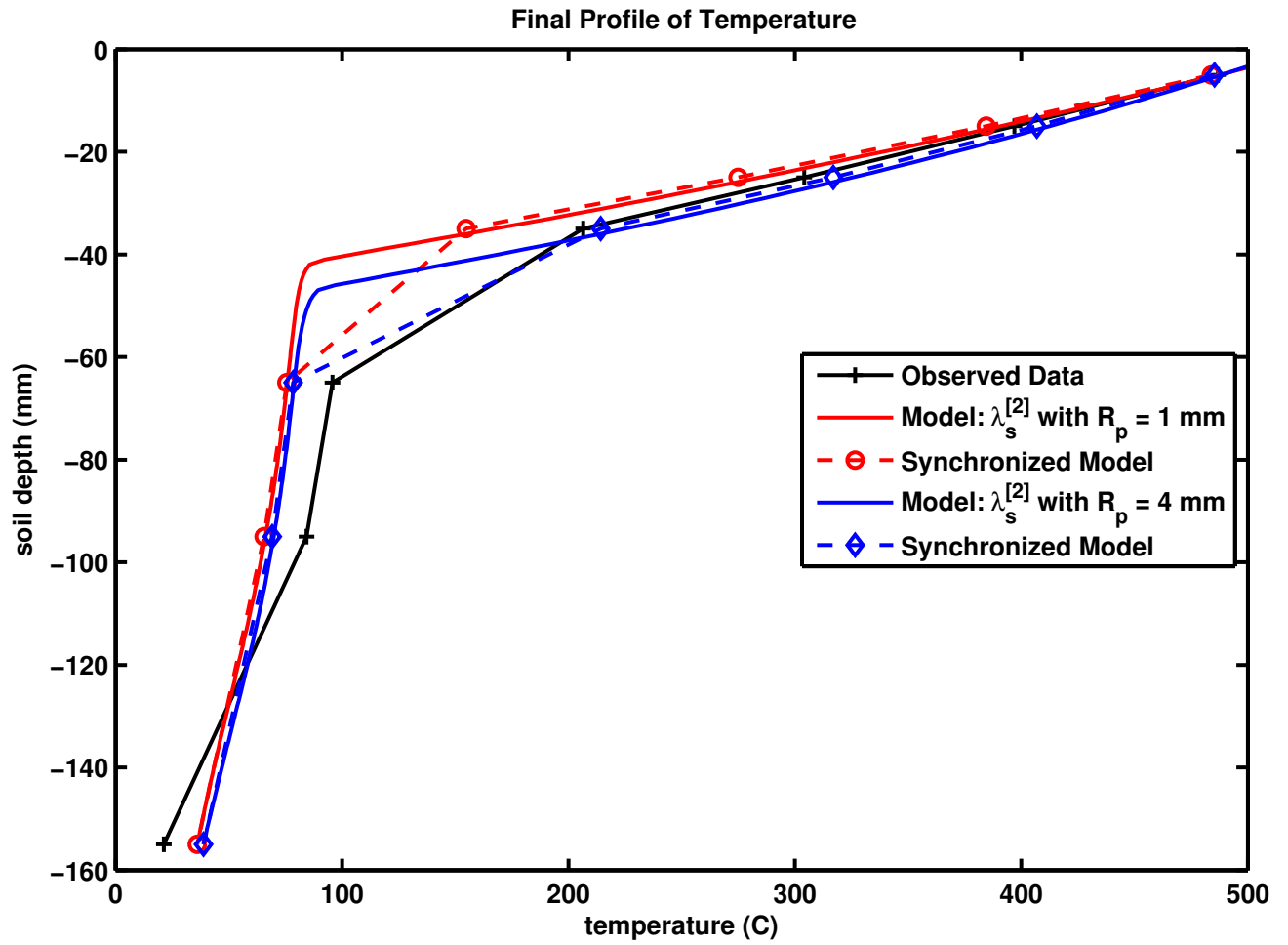


Figure 5:

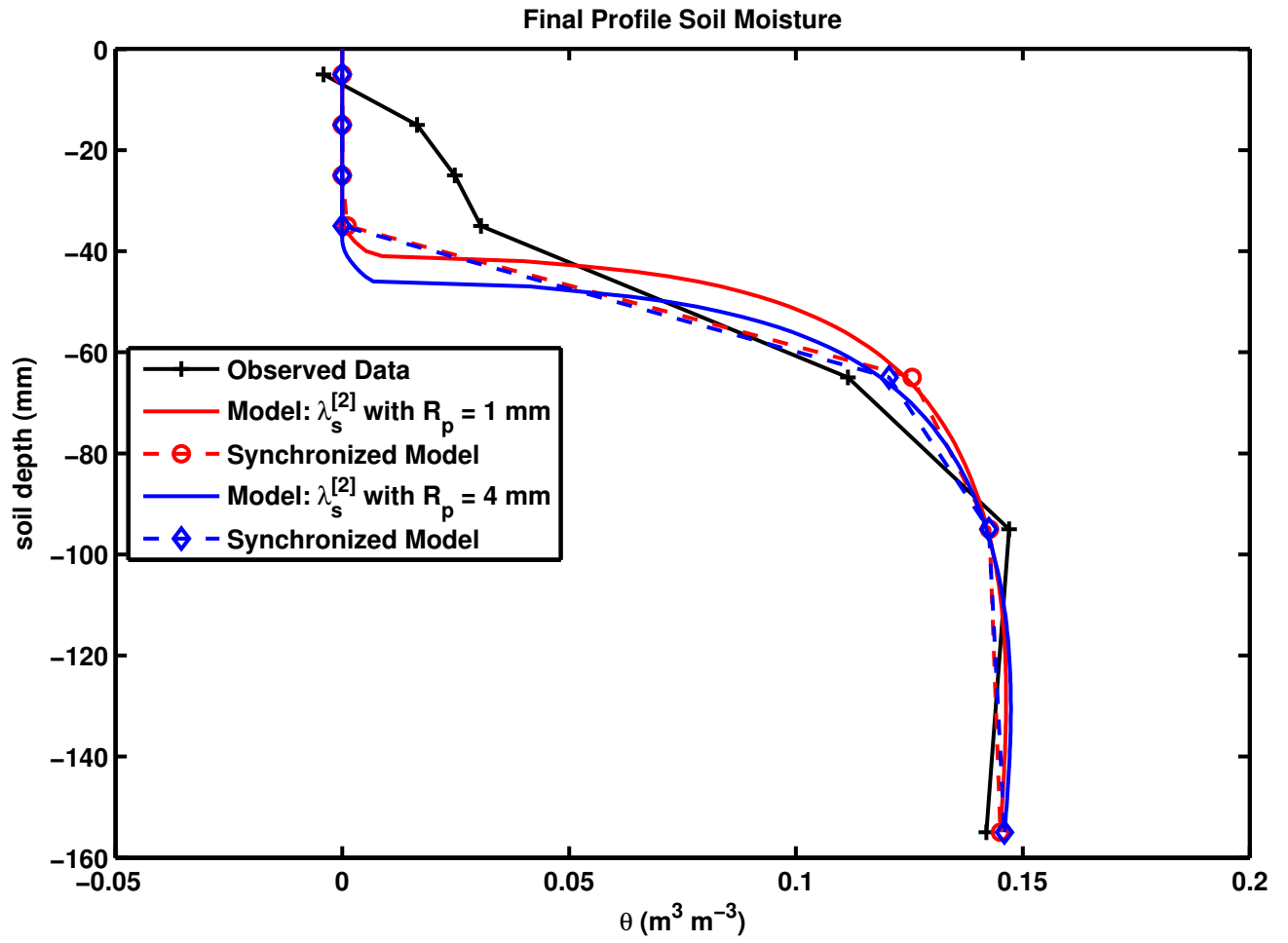


Figure 6:

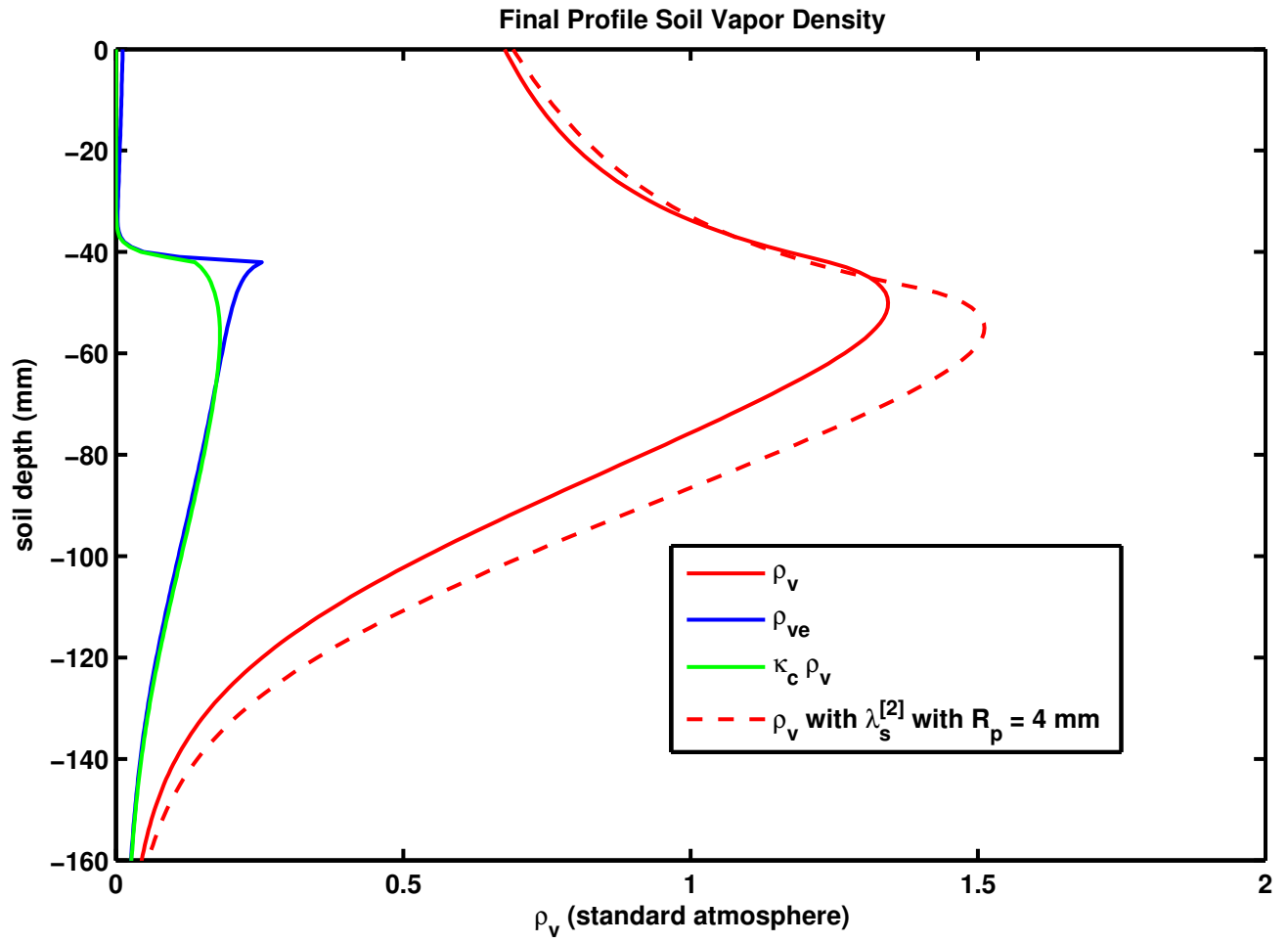


Figure 7:

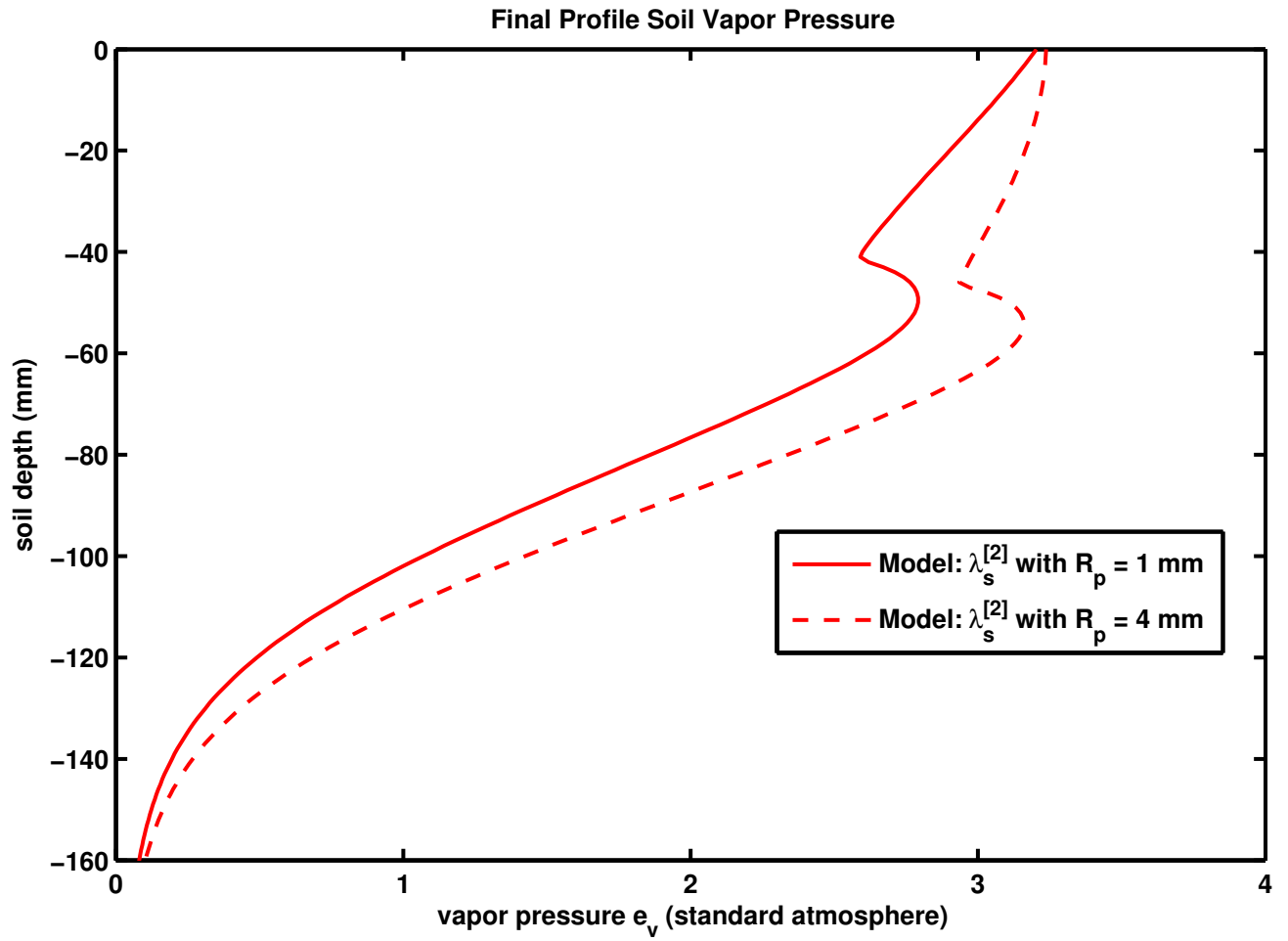


Figure 8:

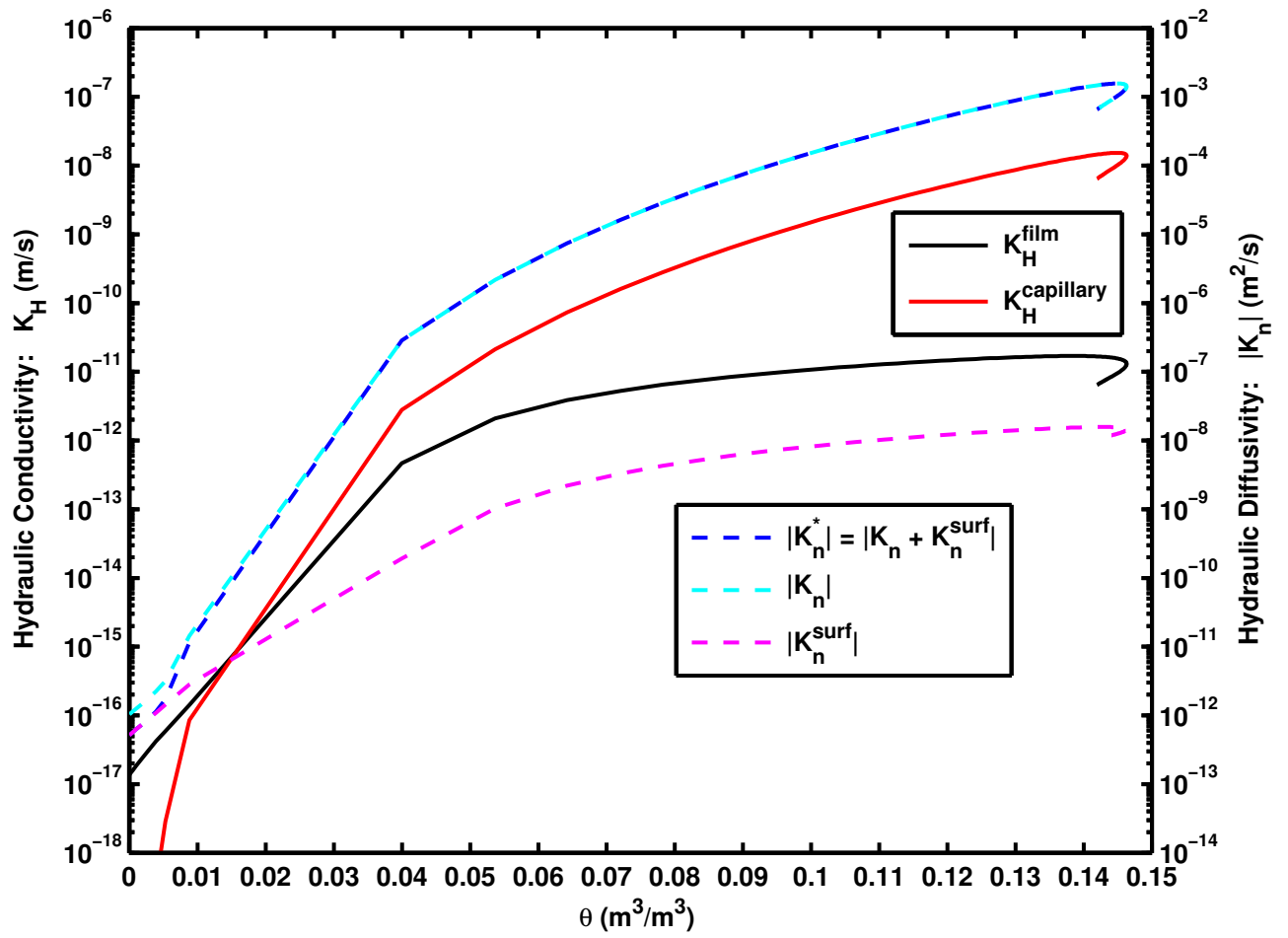


Figure 9:

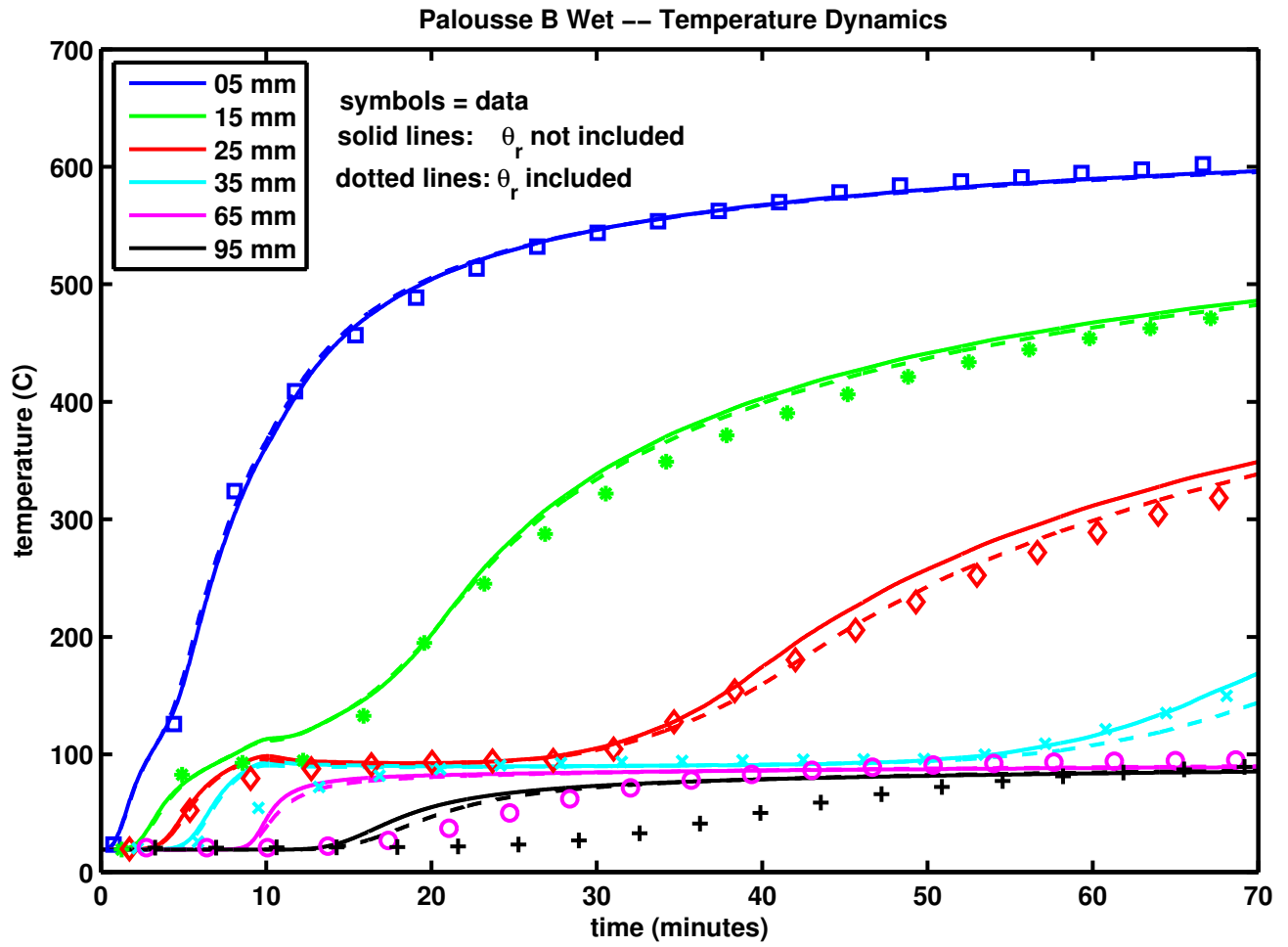


Figure 10:

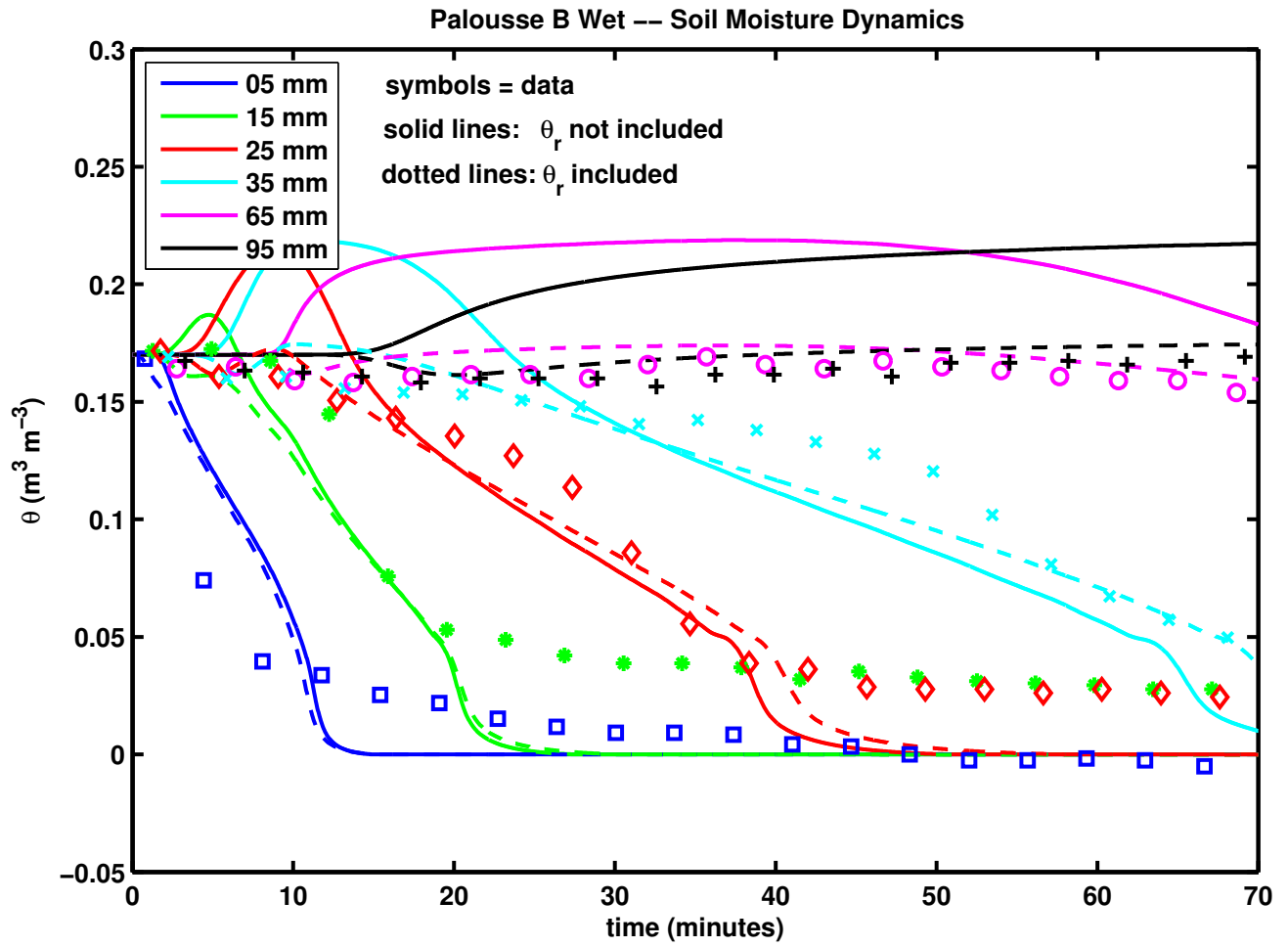


Figure 11:



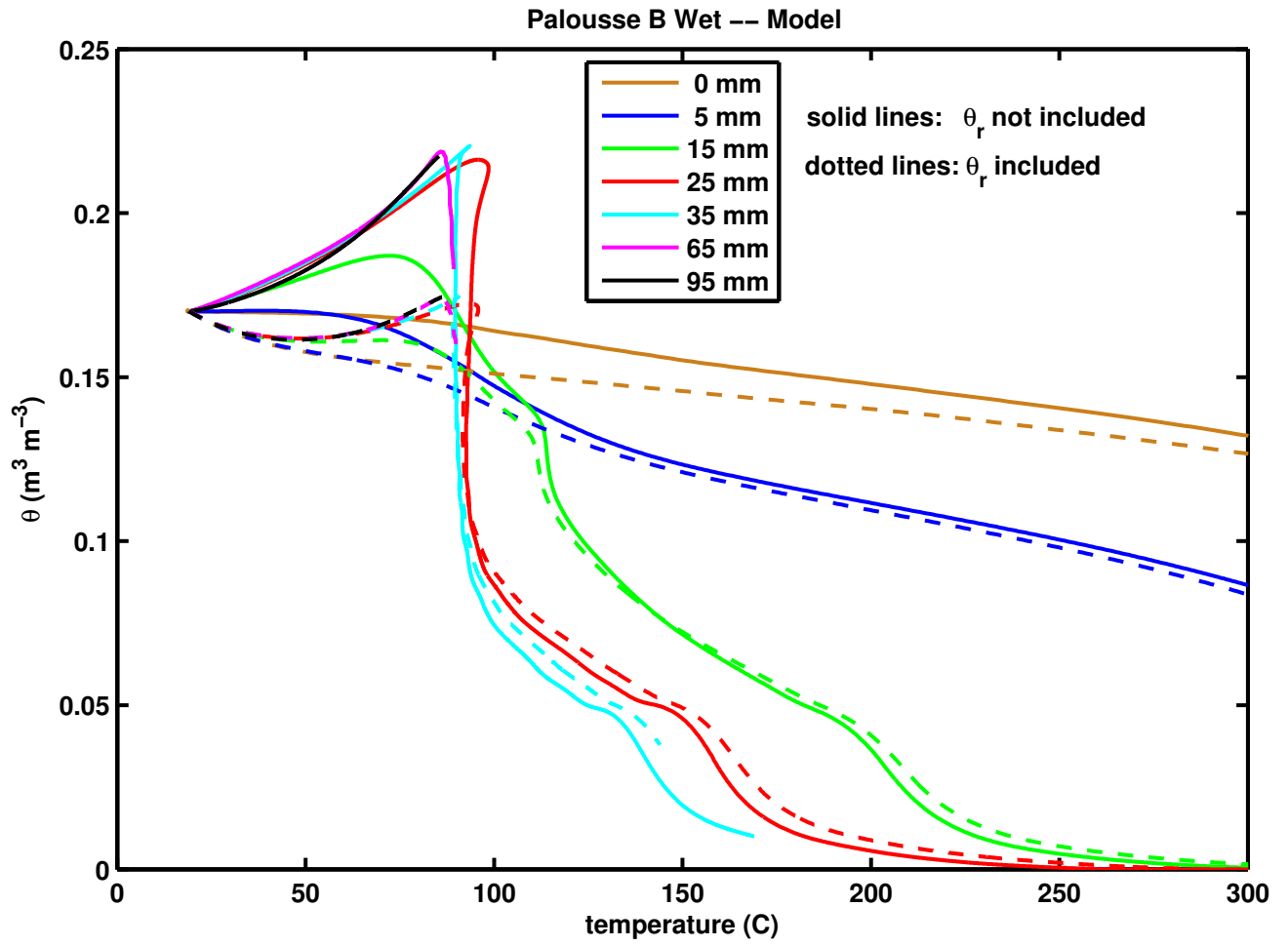


Figure 12:

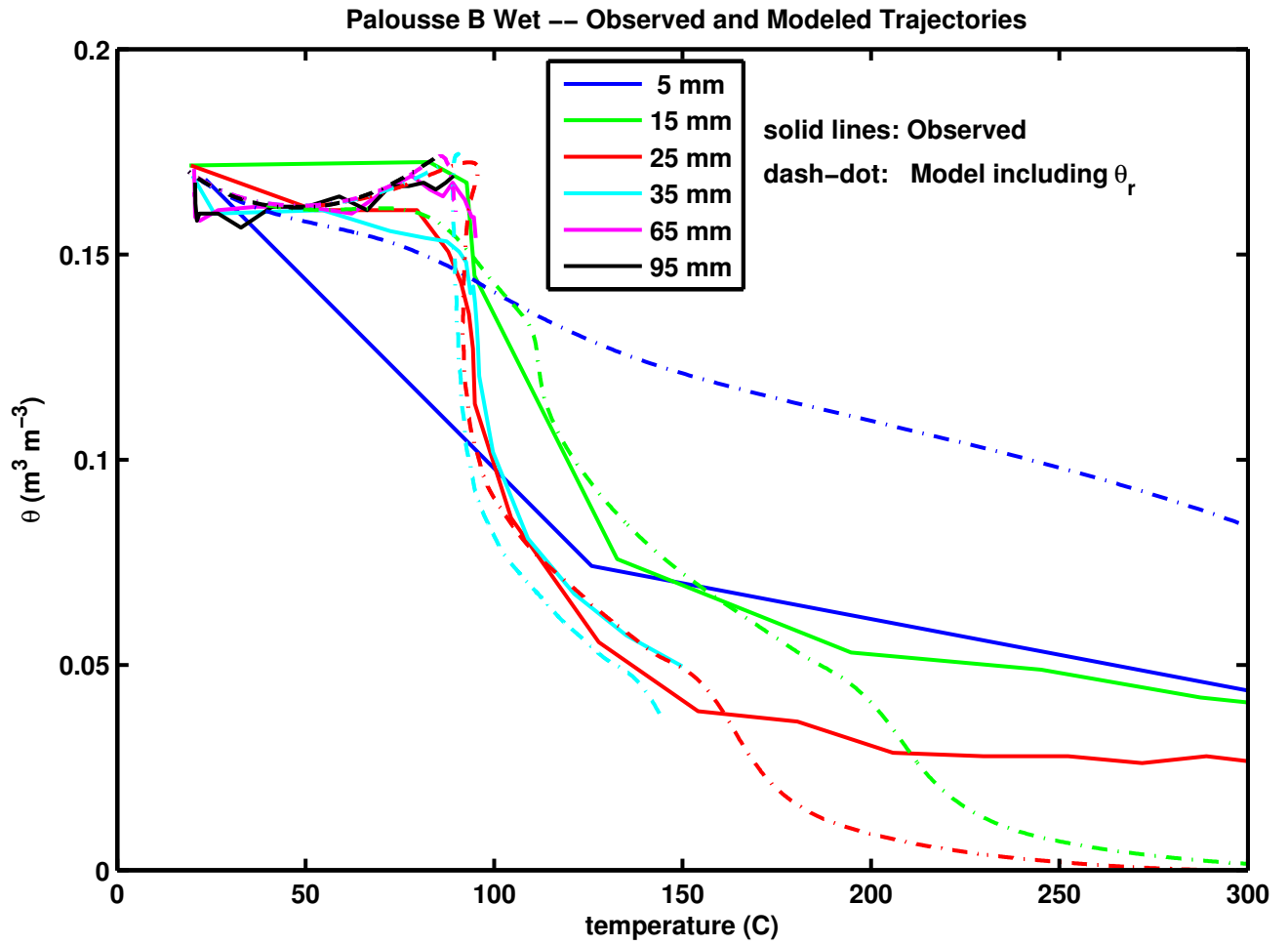


Figure 13:

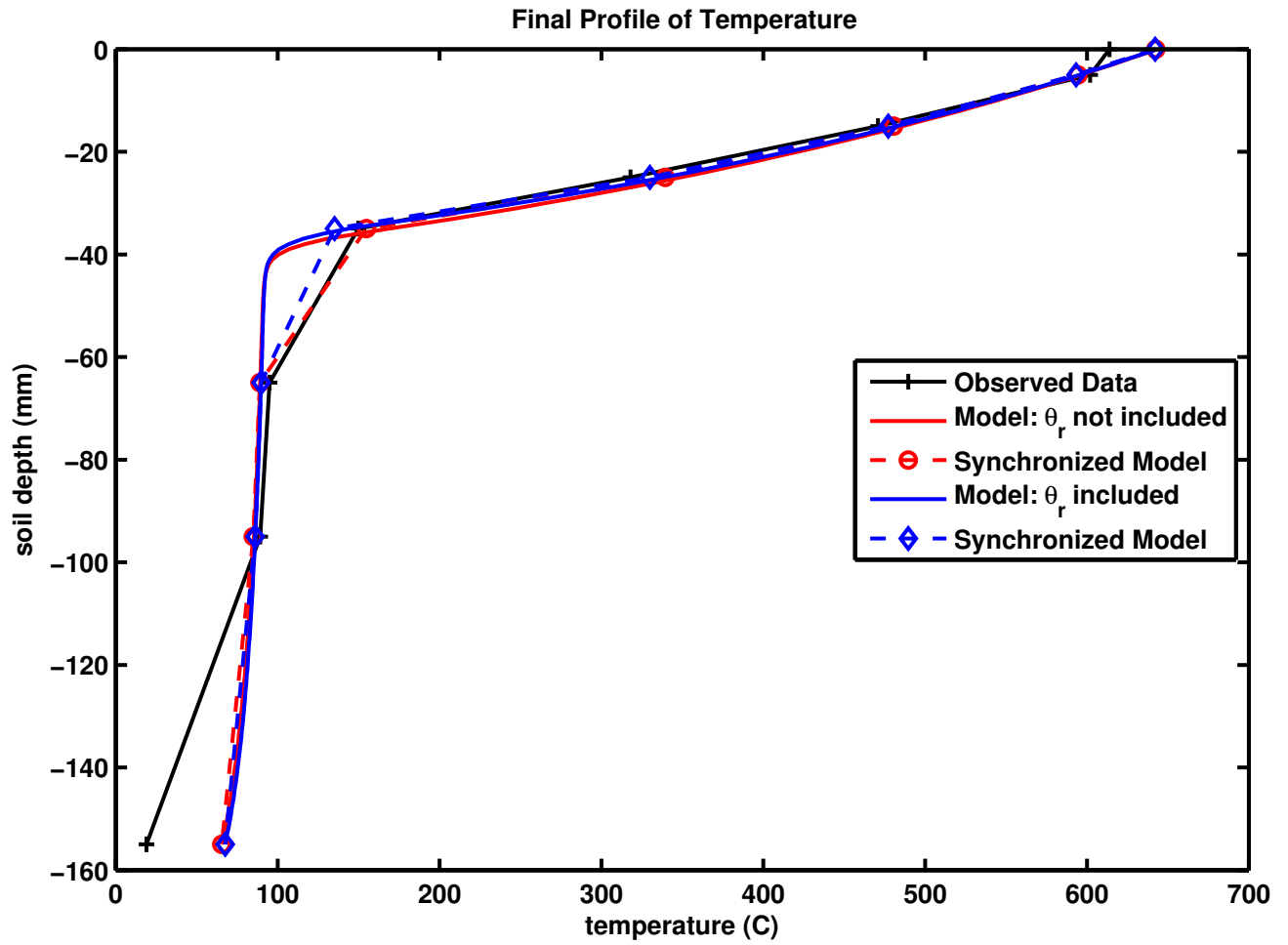


Figure 14:

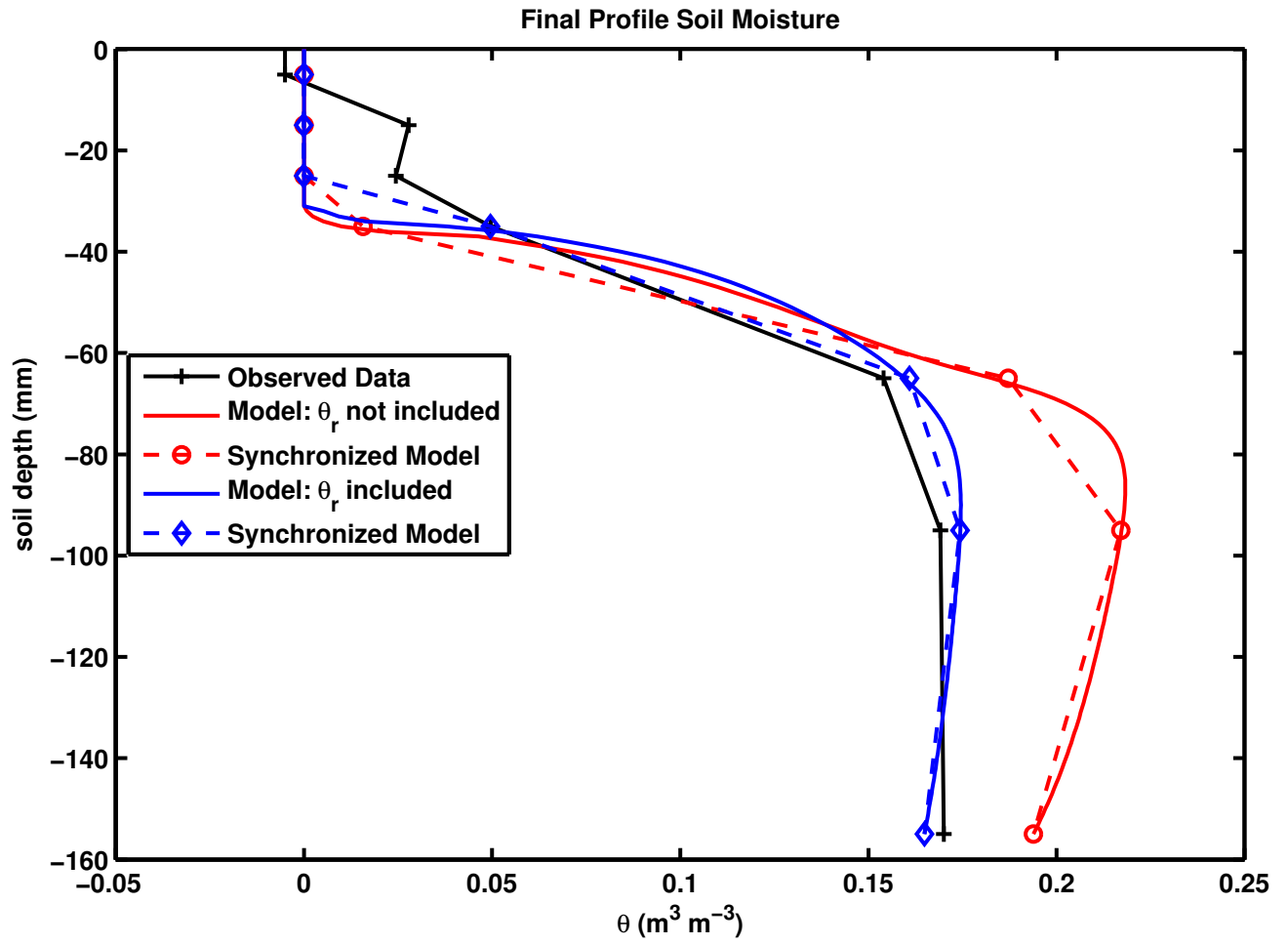


Figure 15:

1144 **Figure Captions**

1145 **Figure 1.** Comparison of measured (symbols) and modeled (lines) soil temperatures during  
1146 the Quincy Sand heating experiment. Neither simulation includes a dynamic residual soil  
1147 moisture term,  $\theta_r$ . The solid lines are for a model simulation with  $R_p = 1$  mm; the dotted  
1148 lines corresponds to a simulation for  $R_p = 4$  mm. Note as  $R_p$  increases the infrared portion  
1149 of the soil thermal conductivity,  $\lambda_s^{[2]}$ , also increases, in accordance with Equation (14). To  
1150 compare with the equilibrium model see Figure 2 of *Massman 2012*.

1151 **Figure 2.** Comparison of measured (symbols) and modeled (lines) soil moisture contents  
1152 during the Quincy Sand heating experiment. Neither simulation includes a dynamic residual  
1153 soil moisture term,  $\theta_r$ . The solid lines are for a model simulation with  $R_p = 1$  mm; the  
1154 dotted lines correspond to a simulation with  $R_p = 4$  mm. To compare with the equilibrium  
1155 model see Figure 3 of *Massman 2012*.

1156 **Figure 3.** Measured soil moisture vs measured soil temperatures for the Quincy Sand  
1157 heating experiment (see previous two figures).

1158 **Figure 4.** Modeled soil moisture contents vs modeled soil temperatures for the Quincy Sand  
1159 heating experiment (see Figs. 1 and 2 above). The solid lines are for a model simulation  
1160 with  $R_p = 1$  mm; the dotted lines correspond to a simulation with  $R_p = 4$  mm. This is the  
1161 solution space representation of the model's solutions, which are to be compared with the  
1162 observations shown in the preceding figure, Fig. 3, as well as with the equilibrium model  
1163 results shown in Figure 5 of *Massman 2012* .

1164 **Figure 5.** Comparison of the final modeled and measured temperature profiles at the  
1165 completion of the 90-minute Quincy Sand heating experiment. Because the data shown in  
1166 the measured profile (black) are not precisely coincident in time, the full model results (solid  
1167 red and blue lines) were sub-sampled in synchrony in time (and coincide in space) with the

1168 observations. These time-synchronized model profiles are shown as dashed red and blue  
1169 lines. To compare with the equilibrium model see Figure 6 of *Massman* 2012.

1170 **Figure 6.** Comparison of the final modeled and measured moisture profiles at the completion  
1171 of the Quincy Sand heating experiment. Because the data shown in the measured profile  
1172 (black) are not precisely coincident in time, the full model results (solid red and blue lines)  
1173 were sub-sampled in synchrony in time (and coincide in space) with the observations. These  
1174 synchronized model profiles are shown as dashed red and blue lines. The observed data  
1175 (black) suggest that the total water lost during the 90-minute experiment was 31% of the  
1176 initial amount. The (red) model simulation indicated a 31.4% loss and the corresponding  
1177 (red) synchronized-model yielded a 33.8% loss. The (blue) model simulation indicated a  
1178 34.6% loss and the corresponding (blue) synchronized-model yielded a 34.2% loss. Note  
1179 there is very little recondensing soil moisture ahead of the drying front (at about 40-50 mm  
1180 depth), in agreement with Figures 2 and 4 above and in contrast with the equilibrium model,  
1181 Figure 7 of *Massman* 2012, where there was significant recondensation.

1182 **Figure 7.** Final modeled profiles of vapor density  $[\rho_v]$ , equilibrium vapor density  $[\rho_{ve}]$ , and  
1183 the condensation coefficient ( $\mathcal{K}_c$ ) modified vapor density term  $[\mathcal{K}_c\rho_v]$  used with the non-  
1184 equilibrium model source term,  $S_v$ , at the completion of the 90-minute model simulation.  
1185 The three solid lines are for a model simulation with  $R_p = 1$  mm; the single dotted line  
1186 corresponds to a simulation with  $R_p = 4$  mm. The maximum vapor density for these two  
1187 simulations is between about 1.3 and 1.5 times the density of the standard atmosphere (=   
1188  $1.292 \text{ kg m}^{-3}$ ) and is located the near position of the maximum in the vapor source term,  
1189  $S_v$ . This figure can be compared with the equilibrium model result: Figure 8 of *Massman*  
1190 2012.

1191 **Figure 8.** Final modeled profile of vapor pressure at the end of the 90-minute model

1192 simulation. The solid line is the model simulation with  $R_p = 1$  mm and the dotted line  
1193 corresponds to the simulation with  $R_p = 4$  mm. In both cases the maximum vapor pressure  
1194 occurs at the soil surface and/or near the level of the maximum  $S_v$ . For these two scenarios  
1195 the maximum vapor pressure is about 3.2 times the pressure of one standard atmosphere (=  $P_{ST} = 101.325$  kPa).  
1196

1197 **Figure 9.** Example of the hydraulic conductivity,  $K_H$ , and magnitude of the hydraulic  
1198 diffusivity,  $|K_n|$ , as functions of soil moisture,  $\theta$ , for the Quincy Sand  $R_p = 1$  mm scenario.  
1199  $K_H$  corresponds to *Assouline's* [2001] HCF for capillary flow, Equation (17), and *Zhang's*  
1200 [2011] model for film flow, Equation (18). Numerically  $|K_n|$  is just a rescaling of  $K_H$  (see  
1201 Section 2.2.5 for further details) and  $|K_n^{surf}|$  is derived from the *Gawin's* [1999] model for  
1202  $V_{\theta, surf}$  (again see section 2.2.5).

1203 **Figure 10.** Comparison of measured (symbols) and modeled (lines) soil temperature during  
1204 the Palousse B Wet heating experiment. The solid lines are for a model simulation that  
1205 does not include the dynamic residual soil moisture,  $\theta_r$ ; the dotted lines correspond to the  
1206 simulation that includes  $\theta_r$ .

1207 **Figure 11.** Comparison of measured (symbols) and modeled (lines) soil moisture content  
1208 during the Palousse B Wet heating experiment. The solid lines are for a model simulation  
1209 that does not include the dynamic residual soil moisture,  $\theta_r$ ; the dotted lines correspond to  
1210 a simulation that includes  $\theta_r$ . For this experiment the initial soil moisture,  $\theta_{in}$ , is  $0.17 \text{ m}^3$   
1211  $\text{m}^{-3}$ .

1212 **Figure 12.** Modeled soil moisture vs modeled soil temperatures for the Palousse B Wet  
1213 heating experiment (see Figs. 10 and 11 above). The solid lines are for a model simulation  
1214 that does not include the dynamic residual soil moisture,  $\theta_r$ ; the dotted lines correspond  
1215 to a simulation that includes  $\theta_r$ . This is the solution space representation of the model's

1216 solutions.

1217 **Figure 13.** Observed and modeled soil moisture vs soil temperatures (trajectories) for the  
1218 Wet Palouisse B heating experiment. Solid lines are observed data and the dash-dot lines are  
1219 from the model that includes the dynamic residual soil moisture,  $\theta_r$ .

1220 **Figure 14.** Comparison of the final modeled and measured temperature profiles at the  
1221 completion of the 70-minute Palouisse B Wet heating experiment. Because the data shown  
1222 in the measured profile (black) are not precisely coincident in time, the full model results  
1223 (solid red and blue lines) were sub-sampled in synchrony in time (and coincide in space)  
1224 with the observations. These time-synchronized model profiles are shown as dashed red and  
1225 blue lines.

1226 **Figure 15.** Comparison of the final modeled and measured moisture profiles at the comple-  
1227 tion of the 70-minute Palouisse B Wet heating experiment. Because the data shown in the  
1228 measured profile (black) are not precisely coincident in time, the full model results (solid red  
1229 and blue lines) were sub-sampled in synchrony in time (and coincide in space) with the ob-  
1230 servations. These time-synchronized model profiles are shown as dashed red and blue lines.  
1231 The observed data (black) suggest that the total water lost during the 70-minute experiment  
1232 was 28.8% of the initial amount. The (red) model simulation indicated a 14.7% loss and the  
1233 corresponding (red) synchronized-model yielded a 15.8% loss. The (blue) model simulation  
1234 indicated a 27.8% loss and the corresponding (blue) synchronized-model yielded a 29.4%  
1235 loss. Note there is very little recondensing soil moisture ahead of the drying front (at about  
1236 35 mm depth), in agreement with Figures 11 and 12.